AGU PUBLICATIONS

JGR

Journal of Geophysical Research: Planets

RESEARCH ARTICLE
10.1002/2013JE004388

Key Points:
- Fresh impact craters reflect Vesta's unweathered surface composition
- Vesta's surface varies significantly on a local scale
- Distribution of materials is related to the formation of Rheasilvia basin

Correspondence to:
K. Stephan,
Katrin.Stephan@dlr.de

Citation:
Stephan, K., et al. (2014), Small fresh impact craters on asteroid 4 Vesta: A compositional and geological fingerprint, *J. Geophys. Res. Planets*, *119*, 771–797, doi:10.1002/2013JE004388.

Received 7 MAR 2013
Accepted 11 MAR 2014
Accepted article online 20 MAR 2014
Published online 10 APR 2014

Small fresh impact craters on asteroid 4 Vesta: A compositional and geological fingerprint

K. Stephan[1], R. Jaumann[1,2], M. C. De Sanctis[3], F. Tosi[3], E. Ammannito[3], K. Krohn[1], F. Zambon[3], S. Marchi[4], O. Ruesch[5], K.-D. Matz[1], F. Preusker[1], T. Roatsch[1], C. A. Raymond[6], and C. T. Russell[7]

[1]DLR, Institute of Planetary Research, Berlin, Germany, [2]Freie Universitaet Berlin, Institute of Geosciences, Berlin, Germany, [3]Istituto di Astrofisica e Planetologia Spaziali, INAF-IAPS, Rome, Italy, [4]NASA Lunar Science Institute, Boulder, Colorado, USA, [5]Institut für Planetologie, Westfälische Wilhelms-Universität Münster, Münster, Germany, [6]JPL, Caltech, Pasadena, California, USA, [7]Institute of Geophysics, University of California, Los Angeles, California, USA

Abstract Small morphologically fresh impact craters (<10 km in diameter) on Vesta's surface with a photometrically distinct ejecta blanket are expected to represent fresh surface material and thus provide the opportunity to study the composition of the unweathered surface. Dawn-Framing Camera and Visual and Infrared Spectrometer (VIR) data reveal impact craters with bright, dark, and mixed, i.e., partly bright and dark, ejecta existing on Vesta's surface, which not only differ in the visible albedo from their surroundings but also in their composition. Differences in the composition are related to the visible albedo and/or the geographic location of the impact craters. Bright ejecta, only seen in the southern Vestan hemisphere, are dominated by howardite/eucrite-like material as expected for Vesta's upper crust. Dark ejecta associated with dark impact craters are dominated by a strongly absorbing, spectrally neutral compound, supporting an origin from carbon-rich impactors. Few impact craters of intermediate albedo in Vesta's southern hemisphere contain material resembling diogenites, which are expected to exist in the deeper parts of Vesta's interior. The geological settings suggest that the diogenite-like material represents a part of a layer of diogenitic material surrounding the Rheasilvia basin or local concentrations of diogenitic material as part of the ejecta excavated during the latter stage of the Rheasilvia impact event. The spectral differences between eucrite- and diogenite-dominated materials also could be verified due to spin-forbidden absorptions in the visible spectral range, which are known from laboratory spectra of pyroxenes, but, which have been identified in the VIR spectra of Vesta for the first time.

1. Introduction

With an average diameter of about 525 km, Vesta is the second largest object in the main asteroid belt and is expected to exhibit a differentiated interior [*Russell et al.*, 2012a; *Thomas et al.*, 1997b]. Vesta is largely believed to be the parent body of HED meteorites (which consist of howardites, eucrites, and diogenites) [*McCord et al.*, 1970; *McSween et al.*, 2011], an expectation that has been confirmed by the Dawn mission results [*De Sanctis et al.*, 2012a; *Prettyman et al.*, 2012; *Russell et al.*, 2012a]. Eucrites, which crystallized close to the surface, are basaltic in composition and contain mostly Ca-poor clinopyroxene (pigeonite) and Ca-rich plagioclase (anorthite) [*Bowman et al.*, 1997; *Delaney et al.*, 1984]. Diogenites are coarse-grained cumulates formed at depth and are composed primarily of Mg-rich orthopyroxenes, with small amounts of plagioclase and olivine [*Beck and McSween*, 2010]. Howardites represent a complex mixture of extensively brecciated and possibly locally melted diogenite and eucrite clasts and fragments, which sometimes also contain parts of the probably chondritic impactors [*Beck et al.*, 2012; *P. Beck et al.*, 2011; *McSween et al.*, 2011]. These meteorites might be the result of one of the huge impact events that had occurred on Vesta [*Binzel*, 1993], like the one that formed the 460 km wide Rheasilvia basin at its south pole [*Jaumann et al.*, 2012b; *Russell et al.*, 2012a; *Schenk et al.*, 2011], excavating material originating from Vesta's crust down its lower crust/mantle, thus shedding light into the composition of Vesta's interior [*De Sanctis et al.*, 2012a; *Jutzi et al.*, 2012]. Vesta is thought to exhibit an iron-nickel core [*Righter and Drake*, 1997b; *Russell et al.*, 2012a], an overlying olivine-dominated mantle, a lower crust of ultramafic cumulates that probably directly crystallized from a slowly cooling magma ocean (diogenites) [*P. Beck et al.*, 2011; *Bowman et al.*, 1997; *McSween et al.*, 2011], and an upper crust of basaltic flows that extruded onto the surface (eucrites) [*P. Beck et al.*, 2011; *Righter and Drake*, 1997a]. However, some HEDs imply less melting and serial magmatism [*Barrat et al.*, 2010; *P. Beck et al.*, 2011]. It is widely

believed that Vesta's basaltic activity ended within the first 10 million years after its formation [*Coradini et al.*, 2011; *Lugmair and Shukolyukov*, 1998; *McSween et al.*, 2011; *Srinivasan et al.*, 1999; *Zuber et al.*, 2011].

Any morphological traces of Vesta's volcanic past, however, have been erased by eons of impacts and solar wind particle bombardment creating a global regolith blanket of pulverized and metamorphosed brecciated material [*Gaffey*, 1997; *Hiroi et al.*, 1995]. In order to further understand the composition of the upper and lower levels of Vesta's crust, unweathered (i.e., fresh) surface areas, which probably occur only on a local scale, have to be identified and their spectral properties have to be studied with respect to their geological and geomorphological context. In particular, ejecta of small impact craters on airless planetary surfaces usually represent relatively fresh material excavated from the subsurface, which could provide insight into the original composition of the planetary object's crust at local scales.

Between July 2011 and August 2012, the Dawn spacecraft visited Vesta [*Russell et al.*, 2012c] providing new imaging and spectral data of unprecedented pixel ground resolution. Based on this new data set, we present a detailed analysis of the geological and compositional characteristics of morphologically fresh impact craters on the surface of the asteroid Vesta. These fresh impact craters show a distinct ejecta blanket and are smaller than 10 km in diameter. We first give an overview of the available data set (section 2) followed by a detailed description of the methodology, i.e., the image processing including the selection process of the impact craters and the algorithms used for the spectral analysis (sections 3 and 4). Section 5 starts with an overview of the different impact crater classes derived from the crater selection process and continues with a detailed description of their geological and spectral characteristics (section 6). In the final part, we discuss the achieved results compared to previous studies, their relationships to HED meteorites, and their implications for the composition and evolution of Vesta's crust.

2. Overview of the Available Dawn Data Set

The instruments aboard the Dawn spacecraft have mapped Vesta from three different orbital heights: (1) from Survey orbit (2700 km altitude), from HAMO (High-Altitude Mapping Orbit, 700 km altitude), and from LAMO (Low-Altitude Mapping Orbit, 210 km altitude) [*Russell and Raymond*, 2011]. During these phases, Dawn detected Vesta's surface with (1) the Visual and Infrared Spectrometer (VIR) which combines a visible-infrared channel (0.25 to 1.07 μm) and an infrared (0.95 to 5.1 μm) channel with a spectral sampling of 1.8 nm per band and 9.8 nm per band, respectively [*De Sanctis et al.*, 2011]. The VIR instrument not only enables us to link Vesta's surface composition to the HED meteorites [*De Sanctis et al.*, 2012a] but also offers the unique possibility of studying the surface composition on a local scale because of the unprecedented pixel ground resolution of the VIR data (~60 m/pixel). The geological and geomorphological context, which is needed to reveal the origin and the geological (endogenic/exogenic) and geochemical processes that could be responsible for the compositional characteristics of Vesta's surface, is provided by images acquired by the Framing Camera (FC). The camera images are taken using one monochromatic and seven color filters (sensitive in the spectral range between 430 and 980 nm) with a pixel ground resolution up to 20 m/pixel [*Sierks et al.*, 2011].

2.1. VIR Observations

During the Survey Mission phase, the VIR instrument observed more than 65% of Vesta's surface, from the South Pole up to 59.2°N, with a pixel ground resolution up to 0.678 km. The phase angle spanned from 78.4° down to 7.8°. Due to the fact that, upon Dawn's arrival at Vesta, the asteroid's northern hemisphere was in winter season with the subsolar point located at a latitude of 26.7°S, data acquired at latitudes greater than 40°N were generally affected by unfavorable illumination conditions (permanent shadows).

The subsequent HAMO phase allowed Dawn's remote-sensing instruments to investigate Vesta's surface in greater detail. During this phase, VIR observations have a roughly constant pixel ground resolution of 0.178 km, with phase angles between 28.2° and 82.7°. Compared to the Survey phase, the spatial coverage was reduced (latitude range from 69.6°S to 45.8°N) due to operational constraints, and footprints were mostly noncontinuous due to the higher instantaneous speed of the ground tracks.

In order to avoid any misinterpretations due to changes in the illumination conditions, the spectral analysis of the selected impact craters was performed based on VIR observations that were simultaneously acquired to the FC images used here for the geological mapping. The VIR observations are available in a radiometrically

corrected data format with the radiometric calibration performed by the VIR team [*De Sanctis et al.*, 2011]. At the time of our analysis, calibrations artifacts are reported for the wavelength regions below 0.4 μm, in the longer-wavelength part of the VIR-VIS instrument (~1–1.02 μm), around 1.4 μm and 2.5 μm [*De Sanctis et al.*, 2013a]. Consequently, these parts of the spectrum were excluded in our spectral analysis. Following the spectral analysis of these observations, which is described below, the resulting data were map projected according to the corresponding FC images.

The VIR observations show the impact craters of interest with pixel ground resolutions between 0.176 and 0.678 km, which is sufficient to identify impact craters down to a diameter of 0.5 km. However, mapping of spectral variations depending on specific characteristics of an individual impact crater (ejecta, crater wall, and crater floor), which is essential to resolve the processes responsible for the existence of spectral compounds, could only be done for impact craters with a diameter of at least 2 km. Since we limited our analyses to very small portions of the surface, the phase angles of the selected VIR observations only vary between 33.5 and 51.9° limiting the effect of the viewing conditions onto the spectral parameters (see below). Nevertheless, photometric correction of the VIR observations were performed according to *Li et al.* [2013], and both uncorrected and corrected VIR observations were analyzed in comparison to each other.

2.2. Framing Camera Data Set

During the orbital phases, FC mapped Vesta's surface with image scales of ~260 m/pixel in the Survey phase, ~60 m/pixel in the High-Altitude Mapping Orbit (HAMO), and ~20 m/pixel in the Low-Altitude Mapping Orbit (LAMO). In order to analyze the spectral and geological properties of Vesta's surface with respect to the local topography, the HAMO digital terrain model (DTM) derived from Dawn FC Stereo images [*Preusker et al.*, 2012] is used. The Dawn spacecraft arrived at Vesta in its southern summer and performed a complete survey of the south polar and equatorial regions up to latitudes of ~45°N with Survey and HAMO data. The FC and VIR data acquired during LAMO cover Vesta's surface, from 90°S up to ~50°N [*Russell et al.*, 2012b]. Good illumination conditions (incidence angle $<70°$) sufficient for our search for morphologically fresh impact craters are only available up to 45°N, which is equal to 66.8% of the surface [*Roatsch et al.*, 2013]. The geologic mapping here is based on the individual FC images, which are available in a radiometrically calibrated and map-projected format. The processing is described in detail in *Roatsch et al.* [2012]. In addition, we use photometrically corrected clear filter images following the method developed by and described in *Schroder et al.* [2012] to measure and compare the visible albedo of our regions of interest at 0.5 μm.

3. Impact Crater Selection

For our analysis, the FC clear filter images are searched for impact craters that appear geomorphologically fresh. The selection of the impact craters is based on global mosaics of Vesta's illuminated surface produced from the clear filter images [*Roatsch et al.*, 2012, 2013] acquired during the HAMO and LAMO phases with a spatial resolution of 60 and 20 m/pixel, respectively.

The major characteristics taken as indicators that these impact craters are very young are the following: (1) a sharp crater rim, (2) a distinct ejecta blanket and/or rays with a visual albedo that stands out in comparison to the surroundings, and (3) the ejecta and the crater itself showing no sign of superposition by more recent impacts [*O'Brien et al.*, 2011; *Pieters et al.*, 2011a].

With increasing age, the impact craters and their ejecta usually become photometrically less distinct due to space weathering processes such as solar wind particle irradiation and/or the progressing mixing with the surrounding material caused by more recent impacts [*Pieters et al.*, 2012a]. Especially in the case of relatively small impact craters, and, consequently, of relatively thin ejecta blankets, the ejecta should fade away after several million years. Therefore, we restricted our analysis only to impact craters with diameters smaller than 10 km, with the assumption that their ejecta deposits represent either excavated subsurface material or remnants of the impactor, and are more or less unaltered by space weathering effects. The amount of impactor material retained in the ejecta material strongly depends on the velocity of the impact. Impacts at Vesta by Vestoids are expected to be relatively slow with a mean velocity of 3.37 km/s [*O'Brien et al.*, 2011], which enables that at least parts of the impactor material could be retained in the ejecta material [*Reddy et al.*, 2012b] and possibly could be identified and distinguished from in situ material during the spectral analysis process.

4. Spectral Analysis Tools

Algorithms used for the spectral analysis of the VIR spectra were chosen depending on the preexisting knowledge of Vesta's surface composition as derived from telescopic spectra and laboratory studies of HED meteorites [*McCord et al.*, 1970; *McSween et al.*, 2011] as well as from initial results of the Dawn mission [*De Sanctis et al.*, 2012a]. The major aspects essential for the spectral analysis are briefly summarized in the following.

It is expected that all VIR spectra of the ejecta material(s) are dominated by the spectral signature of pyroxenes, the most ubiquitous mineral on Vesta's surface [*De Sanctis et al.*, 2012a; *Gaffey*, 1997; *McCord et al.*, 1970]. The most prominent pyroxene absorptions near 1 and 2 μm (commonly referred to as BI and BII, respectively) [*Cloutis and Gaffey*, 1991; *De Sanctis et al.*, 2012a] are caused by spin-allowed crystal field transitions in ferrous iron located in the M2 crystallographic site of pyroxenes [*Cloutis and Gaffey*, 1991]. Weaker absorptions, which occur in the visible spectral range, are caused by spin-forbidden crystal field transitions [*Burns et al.*, 1972; *Klima et al.*, 2007]. The wavelength positions of the pyroxene absorptions, especially the absorptions near 1 and 2 μm are known to be directly related to the pyroxene chemistry, i.e., the amount of Ca and/or Fe within the pyroxene structure [*Cloutis and Gaffey*, 1991]. Both the BI and BII bands shift to longer wavelengths with increasing ferrous iron content. Clinopyroxenes exhibit BI and BII absorptions located at longer wavelengths due to the higher content of Fe and Ca. Orthopyroxenes show BI and BII absorptions at relatively shorter wavelengths as a consequence of more Mg-rich pyroxenes with lower concentrations of Fe and Ca [*Gaffey*, 1976].

HEDs are primarily composed of pyroxenes. Consequently, the wavelength positions for the BI and BII pyroxene absorptions can be used to identify diogenites, howardites, and eucrites [*Gaffey*, 1976]. Usually, the pyroxenes in eucrites exhibit a higher content of calcium and iron (54–60 mol%) than diogenites (20–33 mol %) [*Mittlefehldt et al.*, 1998] and hence have band centers at longer wavelengths than diogenites [*Adams*, 1974; *Cloutis and Gaffey*, 1991; *Gaffey*, 1976]. Howardites, because of their intermediate nature, lie in between but partially overlap the fields of diogenites and eucrites.

In addition, the correlations between band depths and band centers can be interpreted in terms of diogenite/eucrite content of the different Vestan terrains [*De Sanctis et al.*, 2012a]. The depth of these absorptions varies mainly with abundance of the ferrous iron in pyroxenes, the size of pyroxene grains, the absorbing species in the surface material, and with the abundance of any additional opaque surface compounds [*Blewett et al.*, 1995; *Lucey et al.*, 1995; *Tompkins and Pieters*, 1999]. Space weathering also modifies the reflectance spectra and is especially expected to influence the spectral slope from the visible to the ultraviolet wavelength range [*De Sanctis et al.*, 2012a; *Pieters et al.*, 2012a, 2011b; *Tompkins and Pieters*, 1999].

Although diogenites are dominated by orthopyroxenes, a few of them have been found to be rich in olivine [*A. W. Beck et al.*, 2011]. Additionally, the presence of olivine on Vesta has been postulated based on HST and ground-based data by several observers [*Binzel et al.*, 1997; *Gaffey*, 1997]. Recently, olivine has been suggested to occur in very localized regions in the northern hemisphere of Vesta [*Ammannito et al.*, 2013; *De Sanctis et al.*, 2013b]. Olivine, when associated with pyroxenes, is difficult to identify. Nevertheless, it is possible to detect olivine by its prominent absorption at 1 μm, which is located at slightly longer wavelengths and is significantly wider than the 1 μm absorption associated with pyroxenes and thus significantly changes the shape of the pyroxene absorption. Moreover, the presence of olivine has influence on the pyroxene absorption at 2 μm, which is much weaker in olivine/pyroxene mixtures in comparison to pure pyroxene.

Regarding the spectrum at wavelengths longer than 2.5 μm, the mineralogical information that can be inferred is mostly related to the enrichment in OH-bearing (i.e., hydrated) minerals, as revealed by a weak spectral signature at 2.8 μm, that shows up in the dark ejecta [*De Sanctis et al.*, 2012b; *McCord et al.*, 2012]. The spectrum of Vesta's dayside, as measured by VIR beyond ~3.5 μm, is dominated by the thermal emission.

Prominent literature on HED meteorites clearly demonstrates that their mineralogy can be entirely inferred at wavelengths shorter than 2.5 μm. Consequently, the spectral analysis of the selected impact craters in this work focuses on the mafic-silicate absorptions at 1 (BI) and 2 μm (BII) and the visible albedo. This approach is consistent with and enables easy comparison with previous ground- and space-based analyses of Vesta and laboratory studies of HED meteorites. With the aim of being consistent with other studies of Vesta's surface

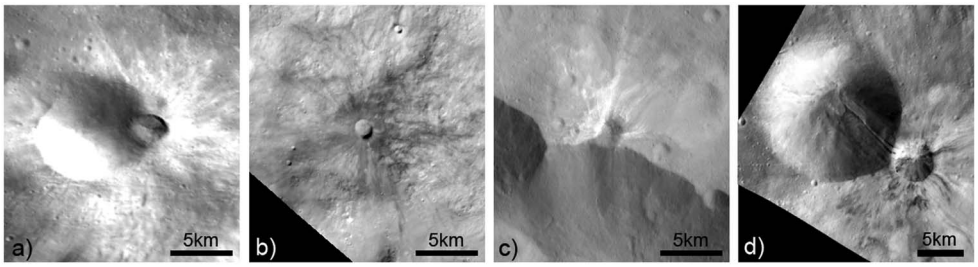

Figure 1. Types of small morphologically fresh impact craters on Vesta's surface: (a) bright crater with bright ejecta, (b) dark crater with dark ejecta, (c) dark crater with bright ejecta, and (d) bright crater with mixed (bright/dark) ejecta.

composition, the spectral parameters were derived following previous work done with VIR data, which concentrated on the spectral mapping of the global spectral variations of Vesta's surface [*Ammannito et al.*, 2012, 2013; *De Sanctis et al.*, 2012a; *Palomba et al.*, 2013]. In these works, the 1 μm absorption (BI) is defined as the reflectance between 0.7 and 1.238 μm, and the 2 μm absorption (BII) is defined as the reflectance between 1.513 and 2.487 μm with the boundaries of the bands chosen to stay away from the calibration artifacts near 1.4 μm and a filter on the focal plane at 2.5 μm [*Ammannito et al.*, 2013]. In order to measure the depth and the wavelength position of these absorptions, the VIR spectra were normalized dividing each spectrum by the corresponding spectral continuum—a straight line between the wavelength start and wavelength stop [*Ammannito et al.*, 2013]. The BI and BII band centers are defined as the minimum of the continuum removed absorptions and the calculation of the band depths follows the definition used first by *Clark and Roush* [1984]. The same methods were applied to HED spectra of the RELAB spectral library, so that both data sets, the HED spectra and our VIR results, can be directly compared to each other.

Reflectance spectra of pyroxenes and olivines are known to vary with surface temperature [*Hinrichs and Lucey*, 2002; *Hinrichs et al.*, 1999], which complicates the derivation of the pyroxene composition out of the VIR spectra. However, specific works carried out for HEDs show that band centers of the pyroxene absorptions will significantly move only upon a large temperature variation [*Reddy et al.*, 2012d]. The VIR data discussed in this work were acquired in a narrow range of local solar times, namely in the Vestan morning between 9.6 and 11 h, and surface temperatures were retrieved by *Tosi et al.* [2012b] for the entire category of bright and dark materials found on Vesta. The temperature difference between the features discussed in the work and laboratory spectra of HEDs is about 50 K in most cases. This implies small shifts in the band centers that fall inside the band center retrieval error and within the average VIR spectral sampling, consistent with the findings by *Ammannito et al.* [2013] and *Reddy et al.* [2012d].

Nevertheless, in order to distinguish changes in the spectral properties of Vesta caused by temperature and composition, we took advantage of the VIR instrument also obtaining spectra in the wavelength region between 3 and 5 μm. The region of the infrared spectrum of Vesta beyond 3.5 μm enables the study of the thermal behavior of Vesta's surface [*Capria et al.*, 2012; *De Sanctis et al.*, 2011]. Thermal characteristics like surface temperature and spectral emissivity were retrieved following the methods described in detail in *Tosi et al.* [2012b, Appendix], in turn updated from *Keihm et al.* [2012, Appendix]. Temperatures were double checked by using also alternative approaches [*Clark et al.*, 2011] as described in detail in *Tosi et al.* [2012a, 2014]. In particular, surface temperature is evaluated in the wavelength range from 4.5 to 5.1 μm. Thermal properties can significantly vary according to physical properties like particle size, rock abundance, bedrock exposure, soil porosity, and regolith thickness, providing complementary information of the surface material, which help to understand the origin of the surface material [*Capria et al.*, 2012].

Spectral properties are analyzed and spectral parameters are derived separately for the defined region of interests based on studying the statistics (mean, max, and average spectrum) of the corresponding VIR data, i.e., for the impact craters themselves, their ejecta deposits, and the surrounding geological units. In order to avoid missing any absorption features related to surface compounds not identified thus far, several algorithms previously successfully applied to identify spectral signatures, such as the calculation of their covariance statistics (especially eigenvectors) as part of the Principle Component Analysis, are used for this study [*Jaumann*, 1991; *Stephan et al.*, 2008, 2010].

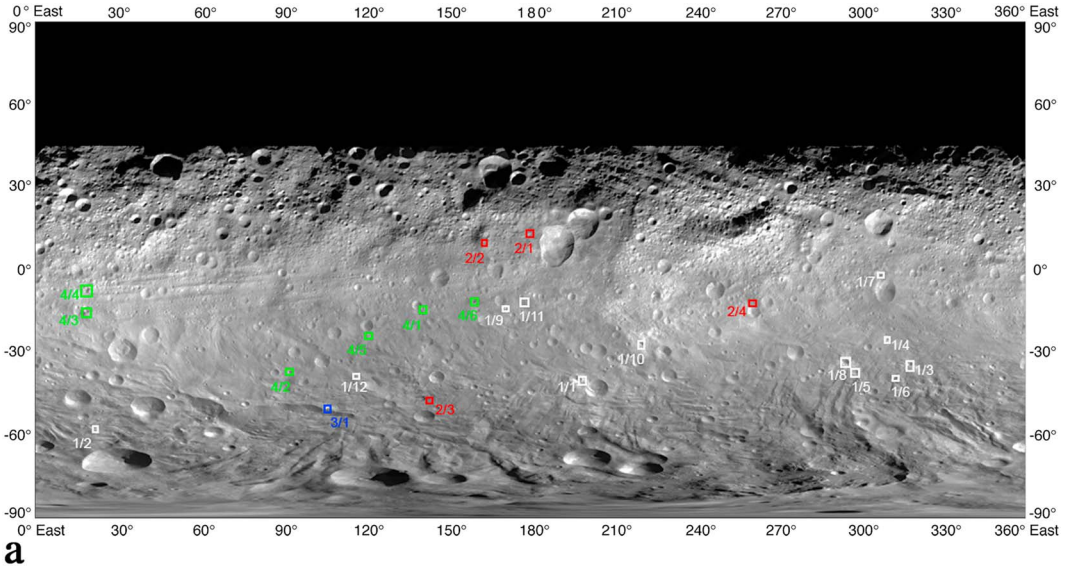

Figure 2. Location of selected impact craters on Vesta's surface on top of (a) a FC clear filter map, (b) the VIR color ratio of the VIR channels at 749/438 nm (Red), 749/917 nm (Green), and 438/749 nm (Blue), (c) Vesta's topography (The black and yellow lines indicate the locations of the Rheasilvia and Veneneia basin near Vesta's south pole), and (d) the photometrically corrected FC clear filter image. The investigated craters are numbered and color coded with respect to the four classes of impact craters (1/1, crater 1 of class 1, white color; 2/1, crater 1 of class 2, red color; 3/1, crater 1 of class 3, blue color; 4/1, crater 1 of class 4, green color).

Moreover, a simple ratio technique provides a powerful tool for discriminating between different spectral classes without the influence of the observation geometry. Several authors [*Isaacson and Pieters*, 2009; *Tompkins and Pieters*, 1999] have successfully used different ratio combinations derived from Clementine images to distinguish between spectrally different surface units, fresh and weathered material, and the varying amount of mafic minerals across a surface on the lunar surface. Particularly, the combination of ratios consisting of images acquired at 415 nm/750 nm and the ratio of the images taken at 750 nm and at a wavelength near 1 μm has been successfully used to study compositional aspects, for example, the freshness and the content of mafic material of the lunar crust [*Tompkins and Pieters*, 1999]. More recently, this ratio technique has been applied to the study of Vesta's surface [*Pieters et al.*, 2011a; *Reddy et al.*, 2012c] using the FC images centered at 749 nm/438 nm (Red), 749 nm/917 nm (Green), and 438 nm/749 nm (Blue). In our study, we use this ratio technique to study spectral variations of the VIR data using the spectral channels acquired at the same wavelength as the FC images, i.e., spectral channels 97 (~438 nm), 252 (~750 nm), and 351 (917 nm). The ratio including the slope from the visible (VIS) to the ultraviolet (UV) spectral range (i.e., from 750 to 438 nm) is used as an indicator for "freshness" of the surface material, and the slope from the visible (VIS) to the near-infrared (NIR) spectral range (i.e., 750 to 950 nm) indicates the depth of the 1 μm pyroxene absorption, which corresponds to the abundance and grain size of mafic minerals, space weathering, and the presence of opaque minerals [*Pieters et al.*, 2012a; *Reddy et al.*, 2012c; *Tompkins and Pieters*, 1999].

5. Derived Impact Crater Classes

Based on these data sets, morphologically fresh impact craters could be distinguished from their surroundings down to a crater diameter of 0.5 km, which thus defines the lower limit of impact craters studied here. The diameters of the selected impact craters do not exceed 10 km. The majority of these impact craters exhibits crater diameters of about 2 km. The impact craters are mostly bowl-shaped and exhibit sharp, fresh crater walls. Their continuous ejecta usually surround the impact crater up to one crater diameter with the discontinuous ejecta, i.e., rays, reaching farther out. Particularly, an asymmetric distribution of ejecta around the crater is often observed, which is probably mostly related to the topography and/or obliquity of the impact event (as discussed below).

As a first cut, the impact craters selected for this study could be distinguished from their surroundings by significant albedo changes (Figure 1). Impact craters exhibiting a significantly higher and lower albedo than

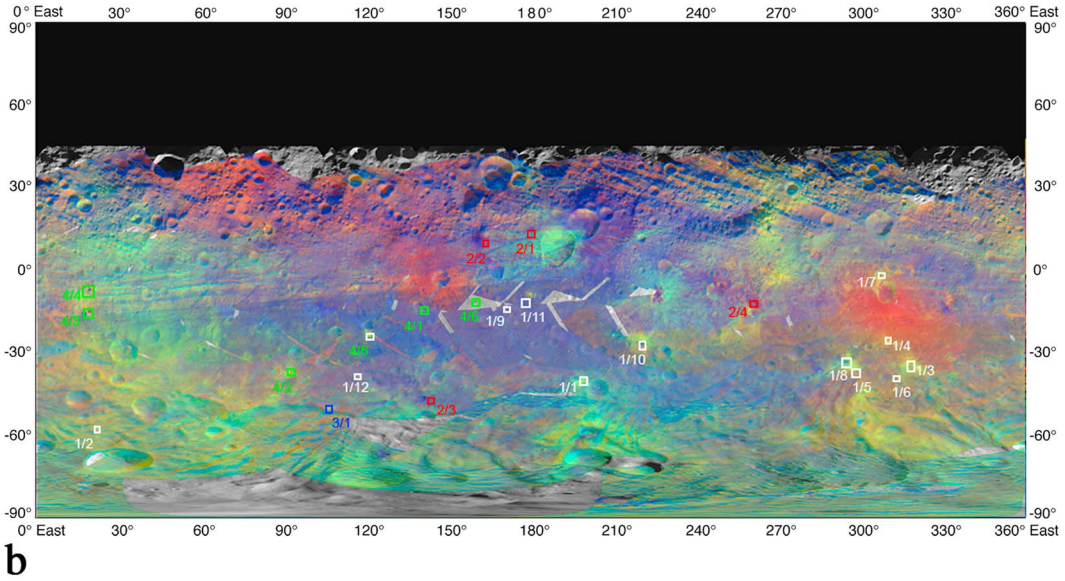

Figure 2. (continued)

their surroundings are apparent. Usually the corresponding ejecta are characterized by a similar albedo. However, impact craters showing different albedo than the corresponding ejecta are also observable. Several craters show bright crater material and dark ejecta, and vice versa. Therefore, the considered impact craters are categorized in the following four groups: (1) bright craters and bright ejecta, (2) dark craters and dark ejecta, (3) dark craters with bright ejecta, and (4) bright craters with dark or mixed (bright/dark) ejecta. Figure 2 illustrates the spatial distribution of the impact craters considered in this study on Vesta's surface.

5.1. Crater Type 1 Bright Craters With Bright Ejecta

Most (i.e., 12 impact craters) of the selected impact craters belong to crater type 1 (Figure 2), which is characterized by a bright crater (crater walls and crater floor) and bright ejecta. Especially, the photometrically corrected FC clear filter images show a high visual albedo (between 0.5 and 0.65) for the ejecta and the impact crater itself (see section 6.1). In addition to the continuous ejecta, rays, which reach relatively far into the distance, are also apparent (Figure 1a).

Since many of these selected impact craters are very small, their detectability is strongly influenced by the pixel ground resolution of the specific VIR observations. FC clear filter images show numerous bright impact craters with diameters smaller than 0.5 km, but, as discussed above, are not included in our analysis due to the restriction of the VIR pixel ground resolution. Nevertheless, impact craters of crater type 1 included in our study were only found in Vesta's southern hemisphere. This means that no bright impact crater with bright ejecta could be identified in the portion of the northern hemisphere that was not hidden during the northern winter. Furthermore, no morphologically fresh impact crater with bright ejecta could be found where the surface shows a higher content of a dark contaminant [*Jaumann et al.*, 2012b; *McCord et al.*, 2012; *Mittlefehldt et al.*, 2012].

5.2. Crater Type 2 Dark Craters With Dark Ejecta

Four impact craters of crater type 2 (Figure 2), which show a dark crater and also dark ejecta, were detected (Figure 1b). The visual albedo of these crater deposits range between 0.22 and 0.14, which is the lowest albedo measured so far on Vesta. There are no obvious albedo changes between the crater itself and the ejecta, which often extend into rays that are visible up to a distance of 5 times the crater diameter measured from the crater center.

These impact craters are detected in the equatorial region between 15°N and 15°S but also far in the south (~50°S) (Figure 2). Usually these impact craters are very small, not exceeding a crater diameter of 2 km. Thus, the low number might result from the fact that most of these impact structures are very small and are not even fully resolved in the FC clear filter images. It cannot be excluded that this kind of impact crater can also be found far in the north.

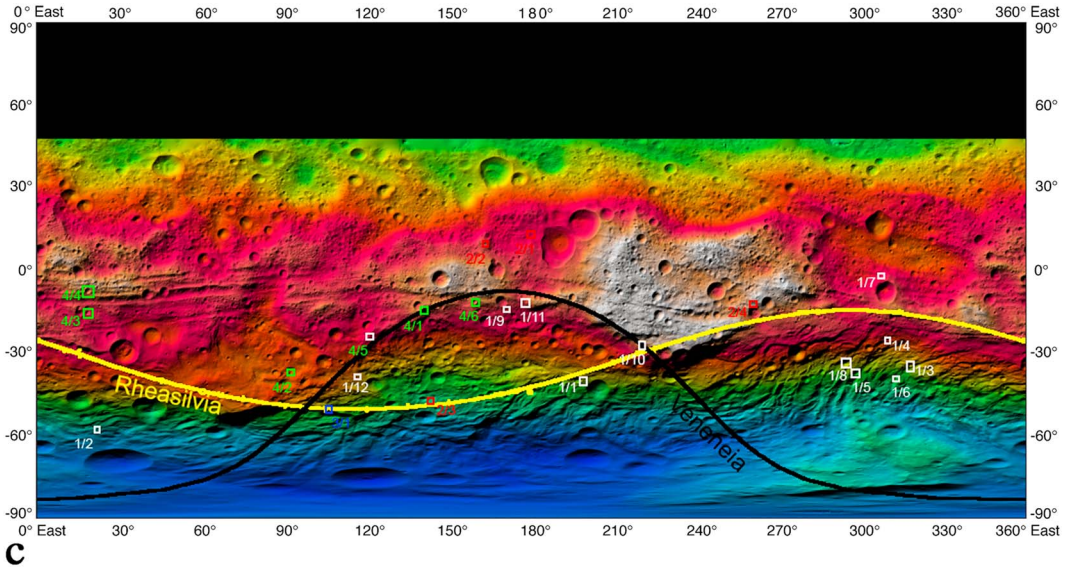

Figure 2. (continued)

Three of the four dark craters with dark ejecta are located in topographically relatively low-lying regions or regions of little or no relief. The exception, Aricia Tholus (impact crater 2/2 in Figure 1 at 10.57°N, 161.2°E) [*Roatsch et al.*, 2012], a dark ray crater on a hill, which represents an impact sculptured rim fragment of an older basin [*Williams et al.*, 2012].

5.3. Crater Type 3 Dark Craters With Bright Ejecta

The impact crater Myia (impact crater 3/1 in Figure 2 at 50.5°S/106.4°E) is the only impact crater of crater type 3 (Figure 1c). The impact crater itself is not as dark as measured for crater type 2, but in the photometrically corrected FC clear filter image, its visual albedo is significantly lower (~0.27) than the bright ejecta extending from the crater especially in the western direction (~0.55) and is still slightly lower than the surrounding region (~0.4). Thus, the impact crater is also defined as dark in this context. Myia is situated at a huge scarp representing the margin of the southern Rheasilvia basin named Matronalia Rupes [*Roatsch et al.*, 2012]. This special location of the Myia impact event probably caused a slump that extends from the crater center down into the depths of the Rheasilvia basin. Both, the impact crater and the slump, show a similar albedo implying a similar composition that might be different from the composition of the bright ejecta.

5.4. Crater Type 4 Bright Craters With Mixed (Bright/Dark) Ejecta

Several impact craters show bright craters and a mix of bright and dark ejecta (Figure 1d). The bright material of the crater itself and the bright ejecta (visual albedo ~0.55) is usually slightly brighter than the surroundings. The albedo of the dark ejecta ranges from 0.25 to 0.37. The ejecta are partly characterized by alternating bright and dark streaks as observed for the impact crater Aelia (impact crater 4/1 in Figure 2) located at 14.2°S and 140.6°E [*Roatsch et al.*, 2012]. In case of an unnamed impact crater at 37.34°S/99.22°E (impact crater 4/2 in Figure 2), the bright ejecta surround this impact crater almost completely and appear to be topographically slightly elevated, compared to the crater rim. Grey streaks extend from the crater center only in the eastwestern direction and reach up to at least 2 times the crater diameter away from the crater. The impact craters of this group are identified only in the southern hemisphere of Vesta, but outside of the Rheasilvia basin, at latitudes reaching from 5°S to 41°S (Figure 2). In a few cases, it is not clear if the dark portions of the ejecta represent freshly excavated material of Vesta's crust or redistributed regolith with a higher amount of probably exogenic dark carbon-rich material. However, the spectral analysis is expected to resolve this question.

6. Spectral Properties of the Impact Crater Classes

6.1. Crater Type 1 Bright Crater and Bright Ejecta

The small impact craters and their corresponding ejecta that exhibit a relatively high albedo in the FC clear filter images (crater type 1) all show a yellow color corresponding to a less steep slope in the ratio color

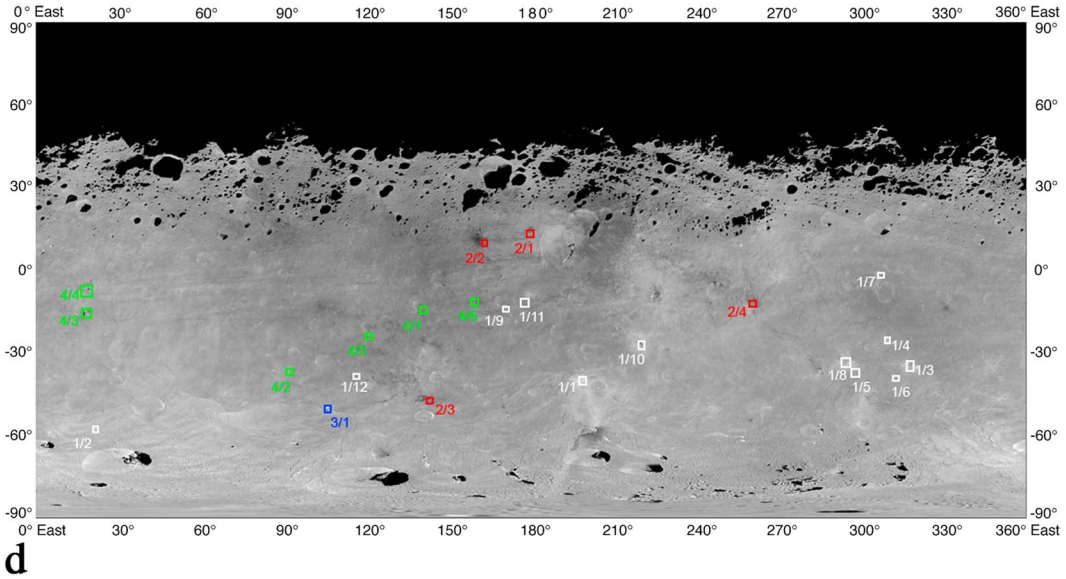

Figure 2. (continued)

composite, indicating that they are fresh. Figures 3 and 4 show a typical example of this crater type (impact crater 1/1 in Figure 2), i.e., a small unnamed impact crater located on the rim of the impact crater Tuccia (39.7°S/198°E) [*Roatsch et al.*, 2012]. This small impact crater is roughly 3.5 km in diameter, and its rayed bright ejecta are distinct up to about 8 km from the crater rim. The VIR spectra of the ejecta of crater type 1, as well as the impact craters themselves, are characterized by a pronounced pyroxene signature (Figure 5). The major pyroxene absorptions in the vicinity of the bright ejecta are, generally, relatively deep. The depth of the pyroxene absorptions ranges between 45 and 55% (BI) and between 22 and 32% (BII). Small variations in the absorptions band depths of the studied bright ejecta of crater type 1 can be explained by differences in the size of the impact crater via the given spatial resolution, i.e., they are not equally resolved in the VIR data and spectral signal from the surrounding regions could be mixed in the same pixel. The wavelength positions of these absorption centers do not change between the different bright ejecta. The absorptions are always centered at 0.94 ± 0.01 μm (BI) and 1.98 ± 0.01 μm (BII), pointing to a relatively high content of Fe [*Klima et al.*, 2007] and therefore to a howardite-like composition with a higher amount of eucrites [*De Sanctis et al.*, 2012a].

Local spectral differences between the ejecta and the crater material are negligibly small. The surrounding regions of the bright crater and their ejecta, which are geologically older and thus have been exposed to space weathering effects, only show a slightly lowered overall albedo, and a slightly less steep VIS-UV slope, as well as weakened BI and BII absorptions (Figures 4 and 5). Again, the positions of these absorptions do not change, implying no change in the pyroxene composition. We therefore infer possible contamination with a

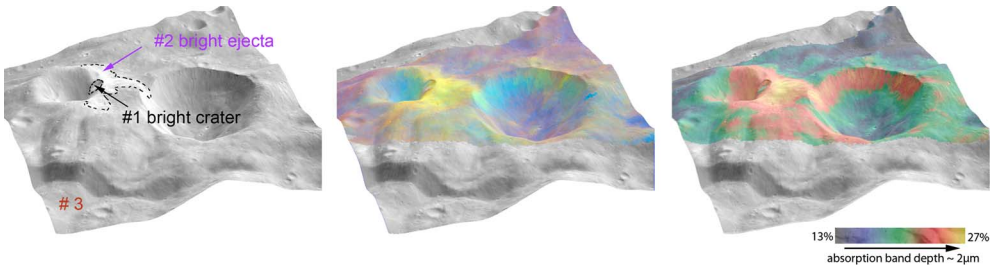

Figure 3. Small fresh bright impact crater with bright ejecta located on the rim of impact crater Tuccia (impact crater 1/1 in Figure 2) (left) by the FC CLEAR filter and (middle) using a ratio color composite of the VIR channels at 749/438 nm (Red), 749/917 nm (Green), and 438/749 nm (Blue), and (right) depth of the BII pyroxene absorption on top of the digital terrain model (DTM).

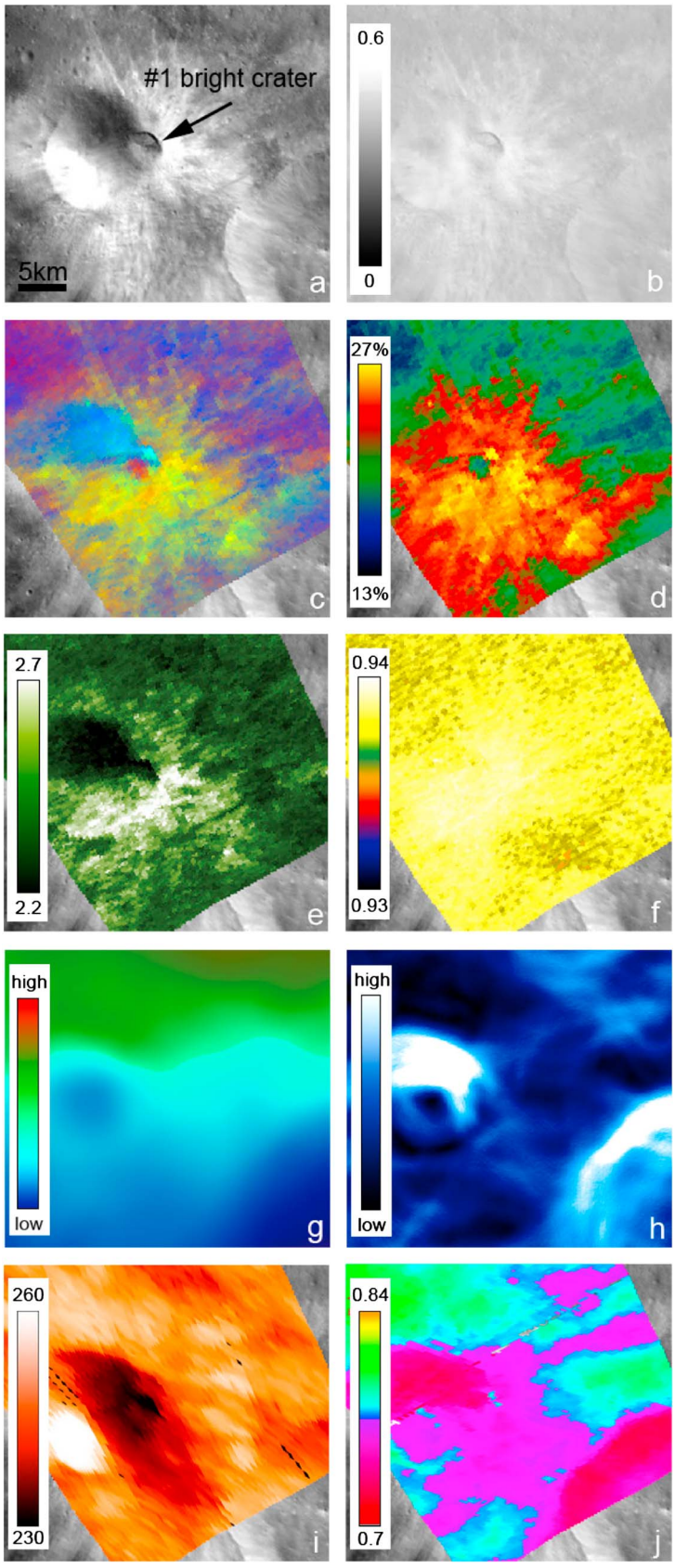

Figure 4

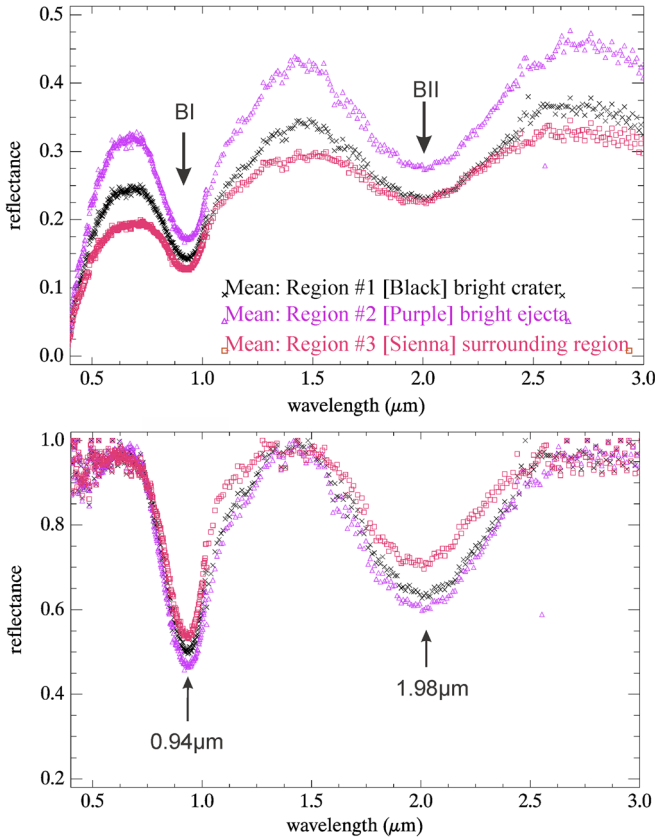

Figure 5. Spectra of ejecta and their surrounding geological units derived for the impact crater shown in Figure 2 as a type example for crater type 1. The spectra are shown (top) before and (bottom) after the normalization to the corresponding continuum. The geological units, which are represented by the spectra, are indicated in Figure 3.

darkening compound (see section 6.2) or a change in particle size to explain the small spectral slope, band depth, and albedo variations. Particle size affects both the reflectance and the band depths.

Additional minor absorptions are expected in the visible spectral range when iron-bearing pyroxenes are present [*Klima et al.*, 2007]. However, no individual or average spectrum shows any indication of these, which either reflects some open issues in the radiometric calibration or these absorptions lying within the noise level of the VIR spectra due to a relatively low signal-to-noise ratio in this wavelength region. The ratio of two VIR spectra, taken from the same VIR observation, however, is a very useful tool for reducing calibration residuals and enhancing small spectral variations between these two spectra. Indeed, the expected features, which are located at 507 and 548 nm and were not reported previously, can be clearly recognized in all ratio spectra of the bright ejecta and their geologically older and weathered surroundings (Figure 6). Other absorptions might exist at 425 and 460 nm. The location of these features supports the existence of iron-bearing pyroxenes on Vesta's surface and fit very well to absorptions seen in the laboratory spectra of hypersthene (especially with particles larger than 50 μm), which is, next to enstatite, one of the typical low-Ca pyroxenes (i.e., orthopyroxene). Spectra of typical high-Ca pyroxenes (i.e., clinopyroxene group: diopsid, augite, and hedenbergite) do not show these features (Figure 7).

The ratio spectrum implies that these features are more prominent in the bright ejecta than in the surrounding regions. This could be explained by effects expected from space weathering processes, which were found to be quite different from that on other airless bodies [*Pieters et al.*, 2012a]. First, the older parts of Vesta's surface

Figure 4. Variations in the changes of specific spectral parameters in the region of the small impact crater shown in Figure 3: (a) FC Clear filter images, (b) photometrically corrected FC image, (c) color-ratio composite as shown in Figure 3, (d) BII absorption depth as shown in Figure 3, (e) VIS/UV ratio, (f) BI band position, (g) local topography, (h) local topographic slope, (i) surface temperature (K), and (j) spectral emissivity.

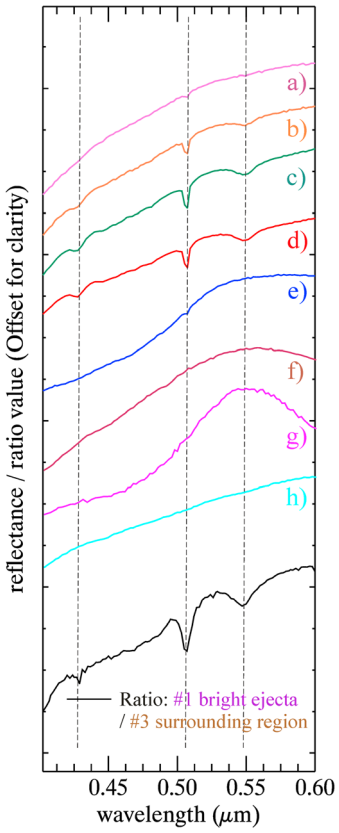

Figure 6. Ratio spectrum enhancing the spectral characteristics of the bright ejecta compared to their "weathered" surroundings (see Figure 5) showing several small absorptions related to Fe^{2+} in comparison to laboratory spectra (U.S. Geological Survey) of orthopyroxenes, i.e., hypersthene of various grain sizes (a) 7, (b) 23, (c) 50, (d) 180 μm, and (e) enstatite as well as clinopyroxenes (f) hedenbergite, (g) diopside, and (h) augite.

are dominated by a layer of well-mixed regolith with an increased amount of dark opaque material derived resulting from large- and small-scale impact events. Second, these low velocity (~5 km s^{-1}) and impacting solar wind particles brecciate and pulverize Vesta's surface material that also could significantly change decrease the particle sizes of the surface material and thus the optical properties [*P. Beck et al.*, 2011; *McCord et al.*, 2012; *Pieters et al.*, 2012a].

Bright ejecta are found to be generally cooler (247 ± 3 K) than the regions surrounding the impact crater (252 ± 3 K) where similar illumination conditions are found (Figures 4i and 4j) and exhibit a relatively low spectral emissivity (0.73 ± 0.12) compared to their surroundings (0.79 ± 0.01). Both measurements are consistent with the high visible albedo of the ejecta reflecting most of the incoming sunlight [*Beck et al.*, 2012]. The lower emissivity might result from the fact that fresh areas like the bright ejecta blanket are not coated with fine regolith resulting from space weathering.

6.2. Crater Type 2 Dark Crater and Dark Ejecta

The dark craters with dark ejecta (Figure 1b) exhibit a relatively low albedo throughout the spectral range of the VIR instrument that is dominated by reflected light (in the spectral region <3 μm). The dark ejecta of the impact crater (impact crater 2/3 in Figure 2; diameter 9.2 km) in the vicinity of impact crater Laelia (46.8°S/140.5°E) [*Krohn et al.*, 2012a] exhibit one of the lowest visible albedos (~0.1) measured on Vesta (Figure 7 and 8). Their spectral properties, however, are still characterized by a distinct pyroxene signature (Figure 9). The wavelength positions of the pyroxene absorptions BI and BII do not change between the bright and the dark ejecta, implying a similar pyroxene composition (Figures 5 and 9). Nevertheless, in the vicinity of the dark ejecta, these absorptions are strongly reduced with respect to their depth—only reaching a maximum depth of about 42 ± 0.5% and 9 ± 1.3%, respectively. Especially, the BII

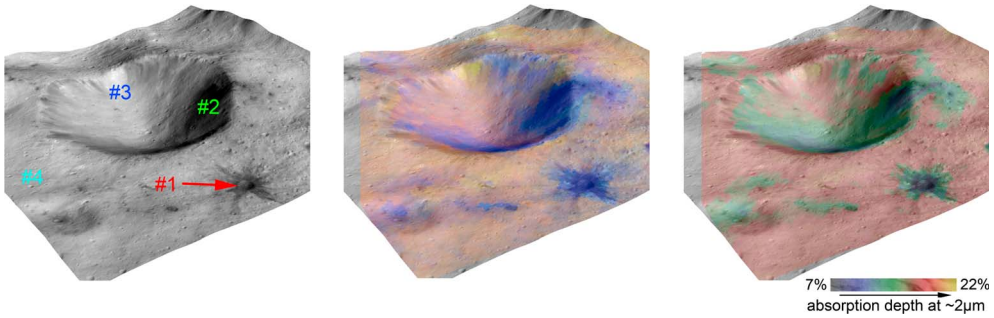

Figure 7. Small fresh dark impact crater with dark ejecta in the vicinity of the impact crater Laelia (46.8°S/140.5°E) as seen by (left) the FC CLEAR filter and (middle) using a ratio color composite of the VIR channels at 749/438 nm (Red), 749/917 nm (Green), and 438/749 nm (Blue), and (right) depth of the BII pyroxene absorption on top of the digital terrain model (DTM).

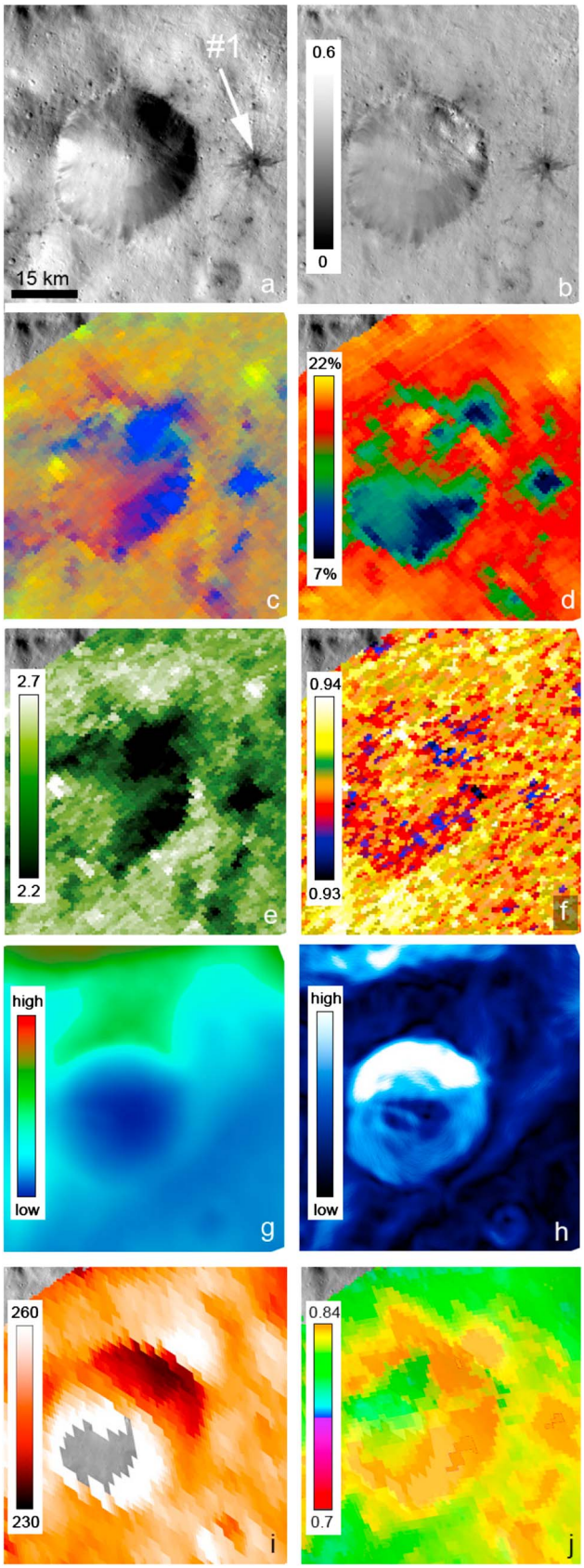

Figure 8

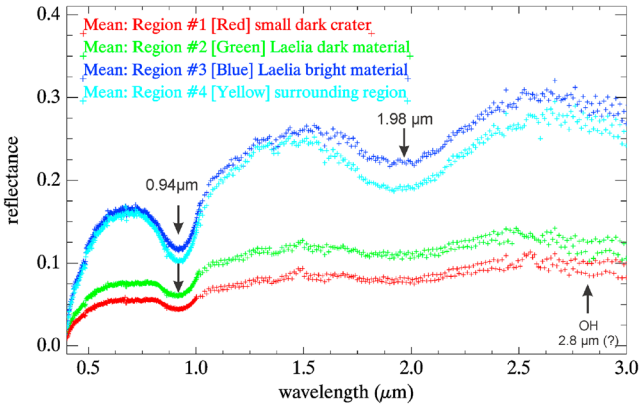

Figure 9. Spectra of dark ejecta and their surrounding geological units derived for the impact crater shown in Figures 7 and 8 as a type example for crater type 2. The geological units, which are represented by the spectra, are indicated in Figure 7. Note the weak absorption near 2.8 µm interpreted by *De Sanctis et al.* [2012b] as the existence of OH in Vesta's surface material.

absorption is barely recognizable in the spectrum of the darkest regions. The ratio indicative of the VIS-UV slope measured for the dark ejecta is slightly lower than measured for the surrounding regions (Figure 8). Therefore, the ratio color composites for the dark impact are dominated by the depth of the BI absorption and the lower VIS-UV ratio—marking the dark crater and ejecta bluish. The spectral properties of the studied dark ejecta appear very similar to each other, are independent of the size and location of the impact crater, and differ only slightly in the depth of the BI and BII absorptions. The slight absorption band variations are likely due to mixing with brighter, pyroxene-rich material, either due to blending of two spatially separated units in the same pixel or more intimate mixing of materials throughout the pixel footprint.

As observed with the impact craters of crater type 1, local spectral differences between the dark ejecta and the crater material are mostly very small. The spectral properties of the brighter surroundings are more similar to the surrounding regions of the bright ejecta of crater type 1 (Figure 9). Ratio spectra of the dark ejecta and their brighter surroundings imply that the surroundings still enclose the small absorptions at 507 and 548 nm, indicative of Fe^{2+} as observed in the bright ejecta (see previous section). The positions of the pyroxene absorptions do not change between the geological units—implying that no changes occur with respect to compositions of pyroxenes. Thus, the spectral analysis of these dark regions suggests an additional darkened but spectrally neutral surface compound reducing and flattening the albedo of the spectral continuum as well as suppressing the pyroxene absorptions. This can be explained if carbonaceous material is present [*Cloutis et al.*, 1990; *McCord et al.*, 2012]. Carbonaceous chondrites are often associated with small amounts of OH^- incorporated into the material. A weak absorption near 2.8 µm can also be tentatively identified in the VIR spectra of the dark impact craters and their dark ejecta (Figure 9), swhich supports the identification of OH^- based on the appearance of a weak absorption at 2.8 µm in the VIR spectra [*De Sanctis et al.*, 2012a].

In contrast to the bright ejecta described above, the surface temperatures derived for the dark ejecta are the highest surface temperatures (257 ± 2 K) and spectral emissivities (0.83 ± 0.12) measured on Vesta (Figure 8). The higher surface temperature can be explained by the low albedo of the dark ejecta, which represent also the lowest albedo measured on Vesta. Higher spectral emissivity is consistent both with the lower albedo and with dark ejecta being made up by very fine particles—even finer than the weathered parts of Vesta's surface.

6.3. Crater Type 3 Dark Crater and Bright Ejecta: Impact Crater Myia (50.5°S/106.4°E)

Although all bright and dark ejecta studied here are found to be dominated by pyroxenes of similar composition, one small impact crater named Myia (impact crater 3/1 in Figure 2) [*Krohn et al.*, 2012a] shows evidence of changes in the pyroxene composition. Figure 10 shows the geological context of the impact crater Myia in comparison with a RGB-color composite using ratios of the VIR channels at 749 nm/438 nm (Red), 749 nm/917 nm (Green), and 438 nm/749 nm (Blue) in a 3-D view based on the topographic data [*Preusker et al.*, 2012]. The impact crater is located at 50.5°S/106.4°E, directly at the rim of Matronalia Rupes, the huge scarp that defines the margin of the southern Rheasilvia basin. The impact crater exhibits distinct

Figure 8. Variations in the changes of specific spectral parameters in the region of the impact crater Laelia: (a) FC Clear filter images, (b) photometrically corrected FC image, (c) color-ratio composite as shown in Figure 7, (d) BII absorption depth as shown in Figure 7, (e) VIS/UV ratio, (f) BI band position, (g) local topography, (h) local topographic slope, (i) surface temperature (K), and (j) spectral emissivity.

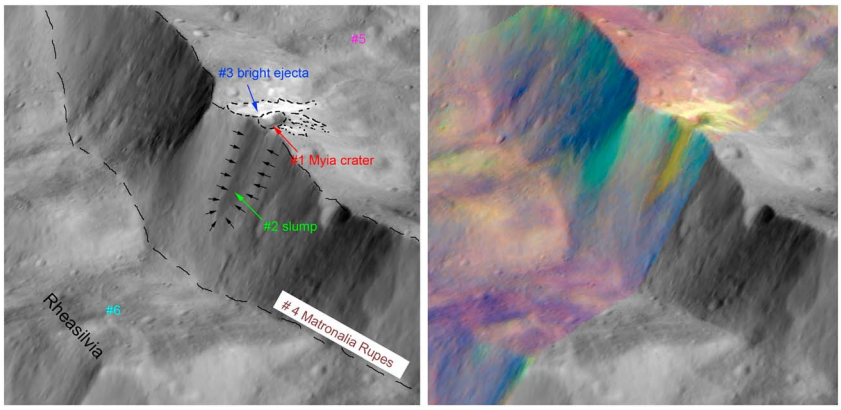

Figure 10. Small fresh impact crater Myia as seen (left) by the FC clear filter and (right) using a ratio color composite of the VIR channels at 749/438 nm (Red), 749/917 nm (Green), and 438/749 nm (Blue) on top of the digital terrain model (DTM).

bright ejecta, which are mainly located along the western part of the crater, i.e., in the region of slightly higher elevation. This uneven distribution of the bright ejecta is probably caused by topography and/or an oblique impact event [*Krohn et al.*, 2012b], or the impactor hit a border between two geological and compositionally different units. The latter hypothesis is supported by the fact that in the clear filter images of the FC camera, the impact crater and the slumping material extending from it is darker than the bright ejecta but is not that different in albedo compared to the surroundings (Figure 11). In the RGB-color-ratio-composite, however, the slumping material appears to be similar in color as the bright ejecta. The yellow color in the color-ratio composite of both the bright ejecta and the slumping material marks both units as fresh (more or less unweathered) material.

Figure 12 shows the average spectra derived for the different geological units in this region. All spectra show the typical pyroxene absorptions BI and BII. The spectrum of the bright ejecta of Myia do not differ from the bright ejecta discussed above with the absorptions getting weaker when moving in the surrounding regions either in the upper or lower region, i.e., outside or inside of the Rheasilvia basin, respectively. The impact crater itself and the material slumping down from the crater along the huge scarp of Matronalia Rupes into the Rheasilvia basin, which are characterized by material with a distinct lower visible albedo, surprisingly shows a spectrum with stronger pyroxene absorptions as measured for the bright ejecta.

Further, the normalized spectra show a significant shift in the position of the BI and BII absorptions. The wavelength position for the BI absorption shifts from 0.94 ± 0.01 μm measured for the bright ejecta and the surrounding regions of the impact crater to shorter wavelengths, i.e., 0.93 ± 0.01 μm, in the vicinity of the impact crater itself and the slumping material. The wavelength position of the BII position shifts from 1.98 ± 0.01 μm to 1.90 ± 0.01 μm. Although these positions are still typical for pyroxenes, they imply changes in the pyroxene composition with respect to the bright and dark ejecta described above, indicating a more diogenite-like composition in the crater and slumping material than in the bright ejecta and their surroundings.

How close these variations appear to be related to the geological/geomorphological units becomes evident when mapping the spectral parameters (i.e., the depth and position of the BI and BII absorption across the region can be seen in Figure 11). The VIS-UV slope, which is also part of the RGB ratio composite as described above, appears to be steepest (which causes the yellow color in the ratio composite) in the vicinity of the bright ejecta as well as in the impact crater and part of the slump. Both major pyroxene absorptions are always relatively strong in all of these geological/geomorphological units, but the average spectra show that they are clearly strongest for the dark crater and the slump. The measured position of the BI absorption separates the crater and slump clearly from the bright ejecta as well as the other geological units. Thus, the absorption positioned at the shortest wavelength is limited to the impact crater itself, the slumping material, and a small part of close-by Matronalia Rupes.

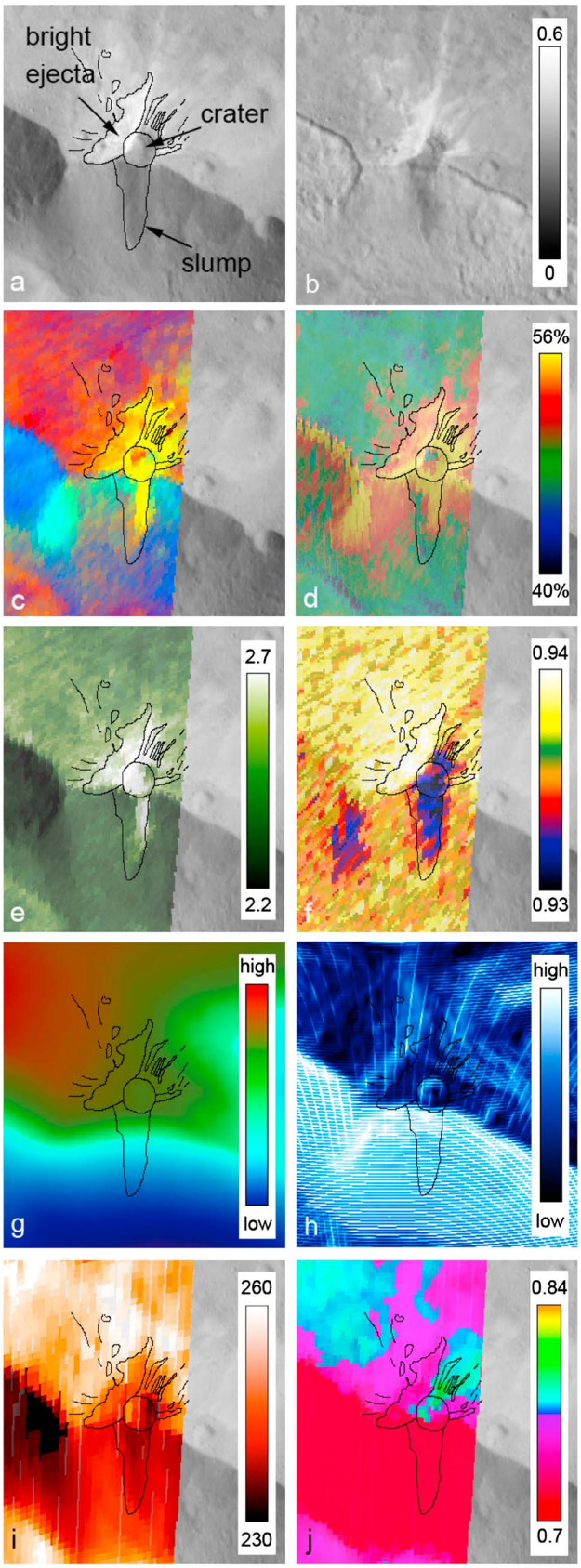

Figure 11

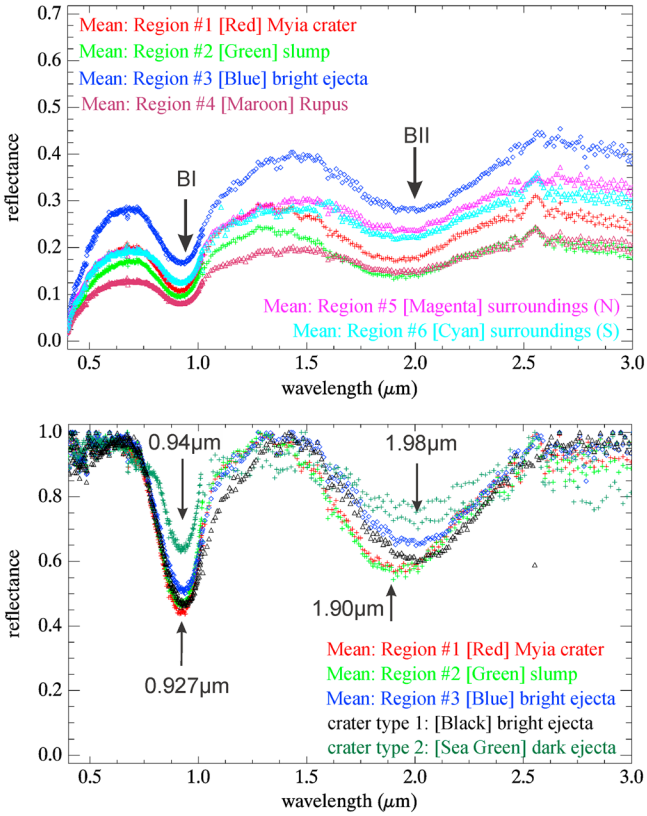

Figure 12. Average spectra of the geological units indicated in Figure 10. Spectra were normalized in order to emphasize changes in the band position of the BI and BII absorptions between the bright ejecta and the impact crater itself and the slumping material extending from it.

The thermal properties of the bright ejecta resemble the bright ejecta of crater type 1, i.e., they show a lower surface temperature (247 ± 3 K) and lower spectral emissivity (0.75 ± 0.13) than their surrounding regions (256 ± 3 K and 0.77 ± 0.2, respectively) where the illumination conditions are similar. The dark crater and the slump are characterized by an even lower surface temperature (236 ± 1 K) and spectral emissivity (0.74 ± 0.06). This contrasts with their relatively low albedo (~0.3). This, however, cannot be explained by albedo alone but support compositional changes implied by the band center changes. The emissivity of the slump and crater is similar to the one of the bright ejecta. But the slump is clearly in a more shadowed region than the bright ejecta, which enhance the temperature differences. The illuminated part of the slump, however, is also cooler than the illuminated part of the Rupes west of the slump—supporting the freshness of the slump material. The slope is equally steep (approximately 35–38°) for the part of Matronalia Rupes imaged in Figure 11. It is only slightly steeper (up to ~44°) in two very limited regions, which corresponds to the slump discussed here but also to an additional region, where the band center of the pyroxene absorption (Figure 11f) also appears at slightly shorter wavelength. The more recent slump is clearly triggered by the Myia impact event. However, both locations enriched in diogenite represent excavated fresh surface and/or subsurface material due to mass wasting processes in regions, where the local topographic slope is to steep that this area could be covered by regolith [*Otto et al.*, 2013].

6.4. Crater Type 4 Bright Crater With Mixed (Bright/Dark) Ejecta

Despite small changes in the albedo and depth of the major BI and BII absorptions, no significant changes in the spectral properties could be measured between the dark ejecta discussed above (crater type 2) and in most of the dark ejecta of impact craters with mixed i.e. bright/dark ejecta (crater type 4). Nonetheless, two impact craters could be identified, which also show changes in the pyroxene composition.

1. Unnamed impact crater (37.34°S/99.22°E)

   Figure 13 shows a small impact crater located at 37.34°S/99.22°E (impact crater 4/2 in Figure 2) with ejecta containing bright and darker material [*Krohn et al.*, 2012a]. Bright material exhibits a slightly higher albedo than its surroundings. In addition, topographically, it appears to be somewhat elevated compared to the crater. Whereas bright ejecta surround the crater almost completely, gray streaks extend from its center only in the eastwestern direction where the surface exhibits a low-lying topography compared to the location of the bright ejecta and most of the crater rim.

Figure 11. Variations in the changes of specific spectral parameters in the region of the impact crater Myia: (a) FC Clear filter images as shown in Figure 10, (b) photometric corrected FC Clear filter image, (c) color-ratio composite, (d) BII absorption depth, (e) VIS/UV ratio, (f) BI band position, (g) local topography, (h) local topographic slope, (i) surface temperature (K), and (j) spectral emissivity.

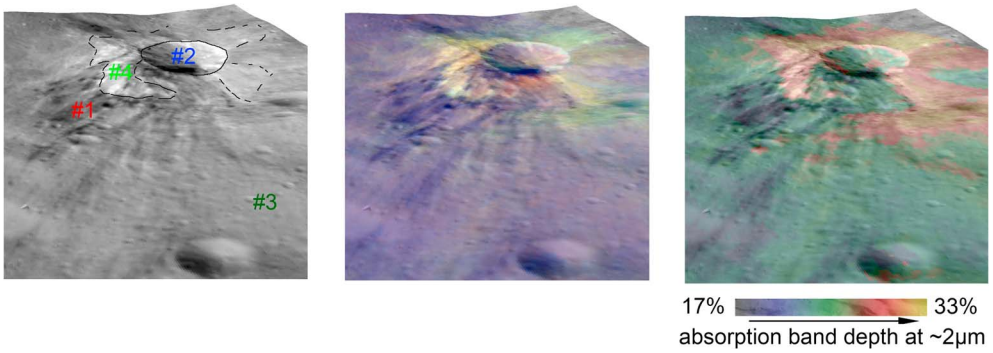

Figure 13. Small fresh impact crater with dark and bright ejecta (37.34°S/99.22°E) as seen by (left) the FC clear filter and (middle) using a ratio color composite of the VIR channels at 749/438 nm (Red), 749/917 nm (Green), and 438/749 nm (Blue), and (right) depth of the BII pyroxene absorption on top of the digital terrain model (DTM).

Ratio color composites clearly separate the crater and the bright ejecta, which appear yellow, from the dark streaks and the surrounding regions, appearing blue (Figures 13 and 14). As described above, this ratio is strongly influenced by the VIS/UV slope, which is steepest in the vicinity of the bright ejecta, and by the depth of the pyroxene absorption BI, which is largest for the bright ejecta. In addition, the wavelength positions of the BI and BII absorptions are similar to pyroxene absorptions at shorter wavelengths in the vicinity of the bright ejecta, which also show the deepest absorptions (Figure 14). The overall shape of the average spectra, as well as the band parameters of the major pyroxene absorptions BI and BII of these ejecta agree with the spectra and parameters extracted and derived, respectively, for the crater Myia and the slump extending from it, pointing to a composition similar to diogenites with a higher amount of orthopyroxenes (Figure 15).

2. Impact crater Aelia (14.2°S/140.6°E)

Figure 16 shows the impact crater Aelia located at 14.2°S and 140.6°E [*Roatsch et al.*, 2012] (impact crater 4/1 in Figure 2) as seen by the FC clear filter image. The impact crater and its ejecta are characterized by bright material with dark streaks. Nevertheless, in the ratio color composite, the impact crater and the ejecta are separated into two spectrally different regions. The border of these units runs through the crater center (Figure 17). Similar variations can be seen in the depth of the major pyroxene absorptions and also in their position, again indicating a change in the pyroxene composition. The deepest pyroxene absorptions, which occur only in the southwestern part of the impact crater and ejecta, also exhibit a wavelength position at relatively shorter wavelengths (0.93 ± 0.01). The average spectrum of this spectral region is similar to the spectrum derived for the Myia crater (see section 6.3) dominated by orthopyroxene (Figure 18). The surrounding region shows a similar spectral signature as measured for bright ejecta of crater type 1. By taking the regional and local topography into account, the southern part of this region shows a strong decline in elevation, marking the margin of the Veneneia basin [*Jaumann et al.*, 2012b] (Figure 2) and pointing to a possible relationship of this basin forming event and the occurrence of diogenite-like material in this region.

7. Discussion: Geological/Geomorphological Interpretation of the Spectral Classes and Implications for Their Possible Origin

7.1. Relationship Between Bright Ejecta and Rheasilvia

VIR spectra show that the pyroxene composition generally does not vary between the different bright ejecta in this study and most of them have a howardite-like composition with a relatively high eucritic component (Figures 19 and 20) [*Zambon et al.*, 2013]. This is consistent with results derived from to the global mapping of Vesta's surface composition [*De Sanctis et al.*, 2012a], showing that howardite and/or eucrite-like composition dominates the equatorial region of Vesta. The composition of the bright ejecta and their exclusive location in Vesta's southern hemisphere supports the hypothesis that the ejecta material represents material initially excavated during the Rheasilvia impact event [*Jutzi et al.*, 2012]. Geologically, they are located predominantly in the so-called Rheasilvia ridge-and-groove terrain, which is interpreted as impact material that forms the floor of the Rheasilvia basin and that was redistributed during the Rheasilvia impact event [*Yingst et al.*, 2012].

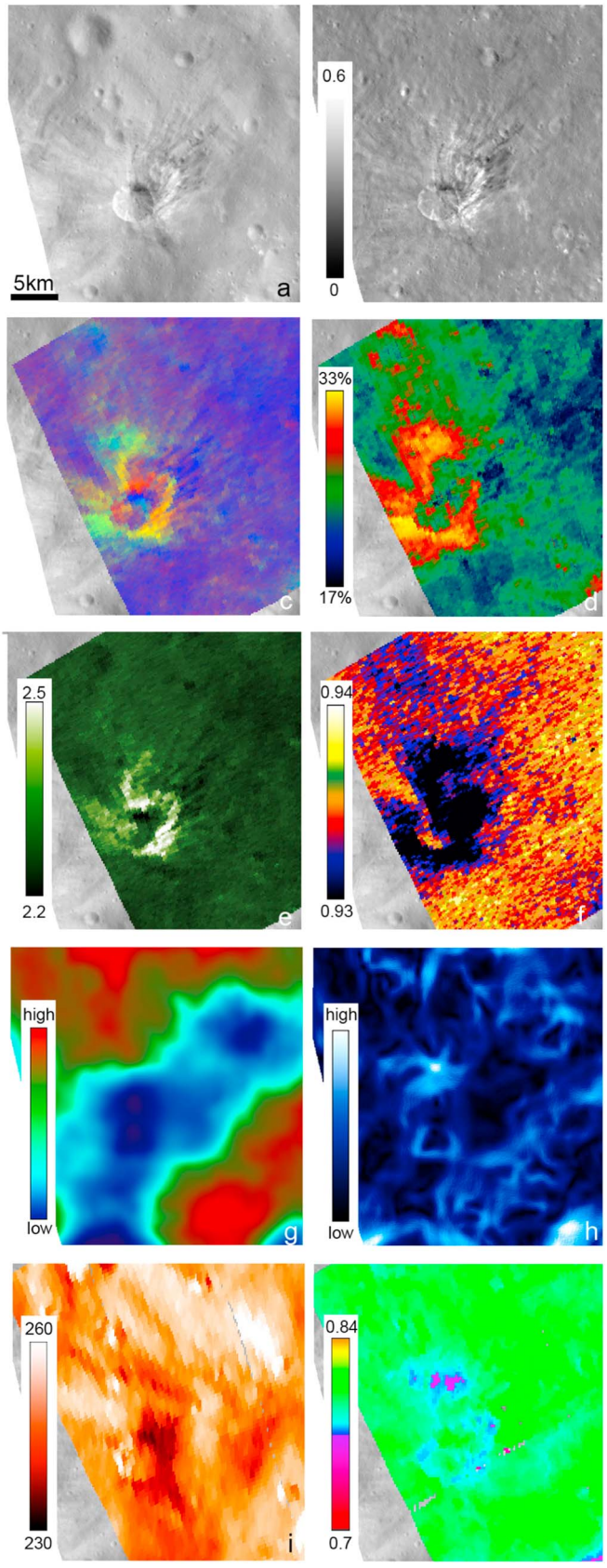

Figure 14

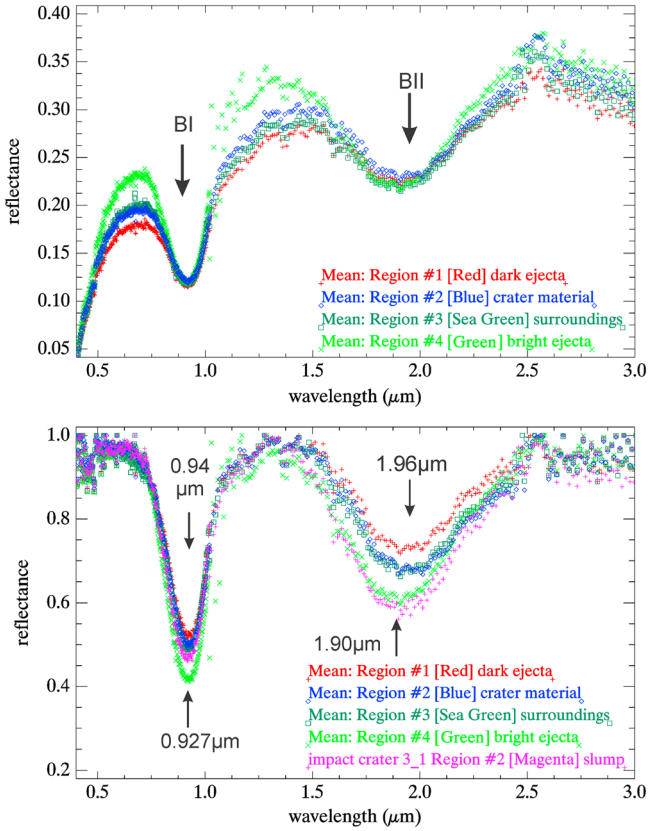

Figure 15. Average spectra derived for the geological surface units as indicated in Figure 13 showing the major pyroxene absorptions BI and BII. Normalized spectra derived for the geological units are compared with the "slump"-spectrum of impact crater Myia (Figure 12).

A few impact craters with bright ejecta, however, also appear in the equatorial cratered terrain [*Yingst et al.*, 2012] but still conform to the expected distribution of Rheasilvia ejecta on Vesta's surface [*Jutzi et al.*, 2012]. Thus, still unweathered portions of this material buried below a layer of regolith are inferred to be reexcavated by the more recent impacts—forming the bright ejecta studied here.

VIR spectra derived from these bright impact ejecta and their surroundings only differ in their overall albedo, between 0.7 and 2.4 μm, and relative strengths of the pyroxene absorptions (Figure 19). Both effects could be explained by changes in the grain size of the pyroxenes and/or a higher amount of dark carbonaceous contaminants in the surrounding regions, which in turn could be related to space weathering due to (micro-) meteoritic impacts, respectively [*De Sanctis et al.*, 2012a; *Pieters et al.*, 2012a].

7.2. Origin of Dark Ejecta Material in Small Impact Craters

Spectra of the dark ejecta show a BI and a BII absorption near 1 and 2 μm, respectively, both of which are strongly reduced but centered at the same wavelength position as measured for the bright ejecta. The dark ejecta are thus consistent with eucrite/howardite-like material mixed with carbonaceous compounds (Figure 19). Despite the suppression of the pyroxene absorptions, no spectral signature can be exclusively associated to the dark ejecta material in the 0.4–2.5 spectral range. Nevertheless, dark ejecta material Vesta has been found to show a weak OH^- signature centered at 2.8 μm [*De Sanctis et al.*, 2012b; *McCord et al.*, 2012]. Certain groups of carbonaceous chondrites show a similar 2.8 μm absorption [*Miyamoto and Zolensky*, 1994; *Takir et al.*, 2011].

Figure 14. Variations in the changes of specific spectral parameters in the region of the impact crater located at (37.34°S/99.22°E): (a) FC Clear filter images, (b) photometrically corrected FC image, (c) color-ratio composite as shown in Figure 13, (d) BII absorption depth as shown in Figure 13, (e) VIS/UV ratio, (f) BI band position, (g) local topography, (h) local topographic slope, (i) surface temperature (K), and (j) spectral emissivity.

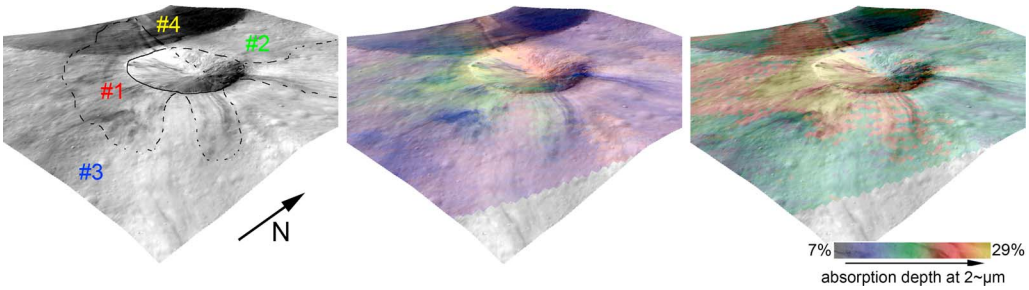

Figure 16. Three-dimensional view of a small impact crater Aelia located at 14.2°S/140.6°E that exhibits two different types of ejecta: (left) FC Clear filter image, (middle) color-ratio composite of the VIR channels at 749/438 nm (Red), 749/917 nm (Green), and 438/749 nm (Blue), and (right) BII absorption.

The appearance of dark ejecta shows no concentration in specific regions on Vesta and thus cannot be related to the Rheaslivia impact event like the bright ejecta. Furthermore, all dark impact craters, which also show dark ejecta, exhibit a crater diameter that does not exceed 2 km and thus cannot have excavated the dark ejecta material from deep down and rather represents redistributed surface regolith or remnants of very low velocity impacts. This findings confirm the predominant association of the dark ejecta material with small impact craters and their ejecta described by *McCord et al.* [2012], who infer an exogenic origin of the dark ejecta material, i.e., representing residuals of carbon-rich, low-velocity impactors, like that found in a major class of meteorites and some comet surfaces [*Gibb et al.*, 2007; *Sandford et al.*, 2006; *Sunshine et al.*, 2006]. The presence of exogenous carbonaceous chondrite meteorite clasts in howardite, eucrite, and diogenite (HED) meteorites from Vesta is well documented [*Zolensky et al.*, 1996]. The infall of carbonaceous material is consistent with the findings derived from previous VIR, GRaND (Gamma Ray and Neutron Detector) and FC measurements [*De Sanctis et al.*, 2013a; *Prettyman et al.*, 2012; *Jaumann et al.*, 2012a; *Reddy et al.*, 2012a].

Similar to the material that makes up the bright ejecta, the dark spectrally neutral (except for an OH absorption at 2.8 μm) material represents one of the spectral end-members characterizing Vesta's surface. The weathered surface surrounding these impact craters shows mostly mixtures of these two materials, due to mixing processes such as impact gardening and transport mechanisms, for example, mass wasting and ejecta emplacement [*Pieters et al.*, 2012b].

7.3. Origin of the Diogenitic Material

The VIR spectra characterized by a distinct shift in the wavelength position of the BI and BII absorption and a slight shift recognizable in the visible absorption at ~0.5 μm toward shorter wavelengths (from 0.507 for howardite/eucrite to 0.505 μm for diogenite) is consistent with diogenitic material (Figure 20), which is known to be dominated by orthopyroxenes [*Cloutis and Gaffey*, 1991]. Diogenitic material associated with ejecta of small impact craters exhibits the deepest pyroxene absorptions measured in our study. This conforms to the higher volume of pyroxenes in diogenites (~90 to 95 vol %) in comparison with eucrites (~50 vol %) [*Bowman et al.*, 1997; *De Sanctis et al.*, 2012a]. It also could imply, however, that the diogenite-like material has a larger average grain size, which is consistent with the theory that Vesta's lower crust composed of diogenites has a coarser pyroxene grain size than eucrites [*De Sanctis et al.*, 2012a; *Mittlefehldt et al.,* 1998]. Although the diogenite-like material exhibits very deep pyroxene absorptions similar or slightly deeper than the Fe-rich bright ejecta, their visual albedo is more or less intermediary (0.28 ± 0.01) in comparison to bright (0.49 ± 0.03) and dark ejecta (0.12 ± 0.01).

In the classical magma ocean, diogenites are expected to occur in the lower crust/upper mantle of Vesta [*Righter and Drake*, 1997b; *Ruzicka et al.*, 1997], which is a significant portion of it excavated during the Rheasilvia event [*Jutzi et al.*, 2013]. This is supported by global spectral maps of Vesta derived from the VIR experiment showing diogenite-rich material as the dominating material in the Rheasilvia basin [*De Sanctis et al.*, 2012a]. The occurrence of diogenite on the surface can be explained as due to excavation during huge impact events like the one that formed Rheasilvia or as representing local magmatic and/or postmagmatic intrusions into the eucrite-dominated Vestan crust as proposed by several studies [*Takeda*, 1979; *Thomas et al.*, 1997a; *Yamaguchi et al.*, 2011].

Diogenitic material associated with ejecta of small impact craters is mainly detected in Vesta's southern hemisphere (Figure 2). In particular, the impact crater Myia is directly located at the Matronalia Rupes, defining

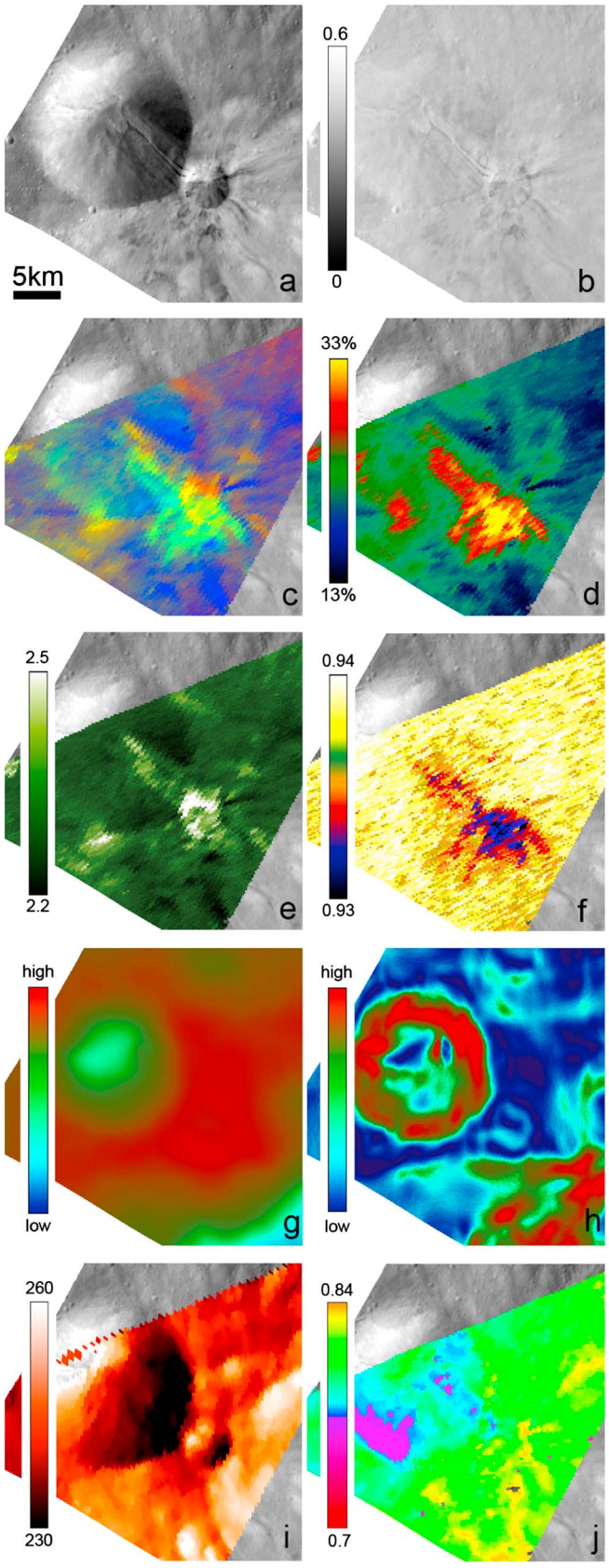

Figure 17

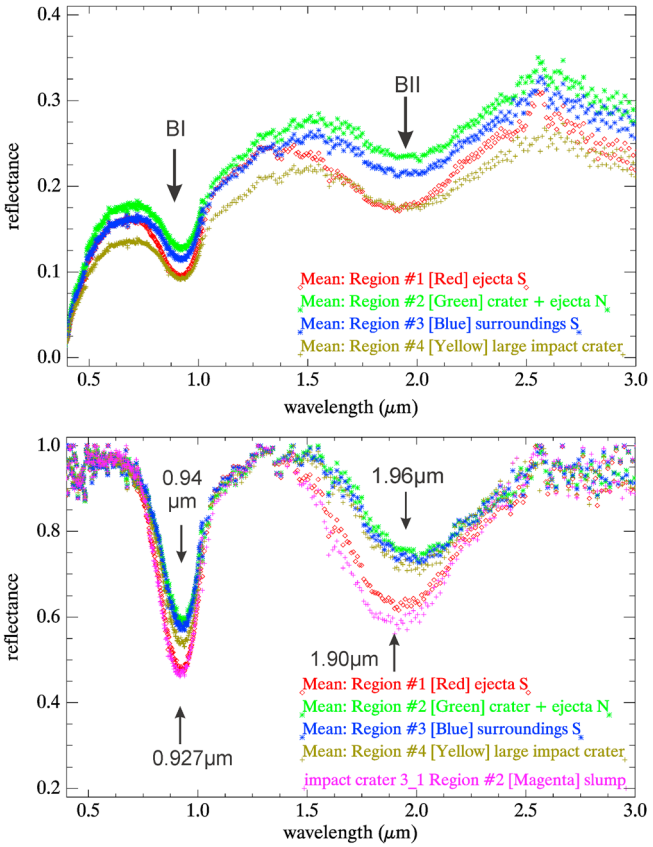

Figure 18. Average spectra derived for the region of the impact crater Aelia as indicated in Figure 16 in comparison to the spectrum of the slumping material of the impact crater Myia (Figure 12) showing the two major pyroxene absorptions BI and BII.

the rim of the Rheasilvia basin. Myia and the slumping material extending from this crater show the highest concentration of diogenitic material detected in the vicinity of small impact craters. Diogenite-like material associated with Myia might represent fresh material from the deeper parts of Vesta's subsurface first having been emplaced during the formation of Rheasilvia and then having been reexcavated during the Myia impact event. Global VIR maps also show a concentration of diogenite-like material in other parts of Matronalia Rupes west of Myia [*De Sanctis et al.*, 2012a], which could imply the presence of a regional layer in Vesta's subsurface close to Rheasilvia itself. Other impact craters with diogenitic material point to small outcrops of diogenitic material, either representing larger blocks of heavily brecciated material excavated in the latter stages of impact events that formed Rheaslivia, or due to the particular location of the impact crater Aelia, Veneneia.

8. Summary

Three different types of spectral end-members are identified characterizing the material of several small fresh impact craters and their ejecta: (1) eucrite/howardite-like material that dominates the bright ejecta of the impact craters of types 1 and 3, (2) visually dark, spectrally neutral neutral (except for an absorption at 2.8 μm), probably carbon-rich material concentrated in the dark ejecta of impact crater type 2, and (3) diogenitic material observed in the special setting of impact crater Myia (impact crater type 3) and in the ejecta of two impact craters of impact crater type 4. These end-members strengthen the findings of previous works [*De Sanctis et al.*, 2012a], thereby linking the chemical composition and mineralogy of Vesta's crustal material to

Figure 17. Variations in the changes of specific spectral parameters in the region of the impact crater Aelia located at 14.2°S/140.6°E: (a) FC Clear filter images, (b) photometrically corrected FC image, (c) color-ratio composite as shown in Figure 16, (d) BII absorption depth as shown in Figure 16, (e) VIS/UV ratio, (f) BI band position, (g) local topography, (h) local topographic slope, (i) surface temperature (K), and (j) spectral emissivity.

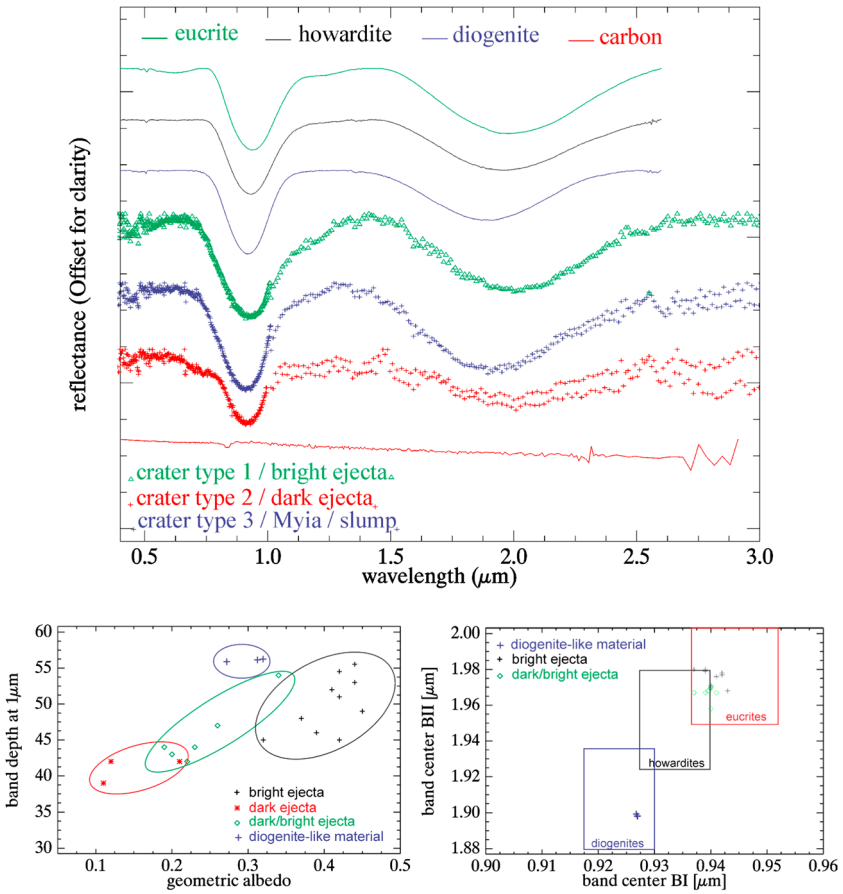

Figure 19. (top) VIR spectra of the spectral end-members (1) bright, (2) dark, and (3) diogenitic material in comparison to laboratory spectra of HED meteorites and carbon as the darkening compound (RELAB spectral library); (bottom left): comparison of the BI absorption band depth of the selected impact crater materials to the visual albedo, and (bottom right): BI and BII band center positions in comparison to the HED laboratory spectra (RELAB).

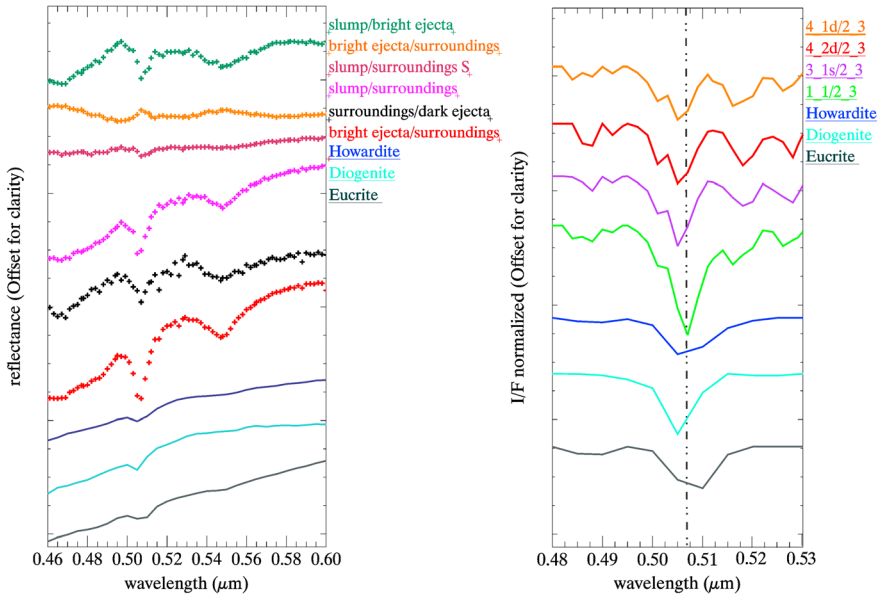

Figure 20. Ratio spectra of the visible part of VIR spectra derived (left) for the specific geological units described in Figure 10 and (right) individual ratio spectra of the derived materials (i.e., 1: bright ejecta, 2: dark ejecta, 3: slump of impact crater Myia, 4: ejecta composed of diogenite-like material) in comparison to spectra of HED meteorites. Note that the spectrum 2_3 of dark ejecta is used as a reference since its spectrum is dark without any small absorptions related to pyroxenes.

the HED meteorites. The spectral differences also could be verified due to changes in the wavelength positions of absorptions in the visible spectral range caused by spin-forbidden crystal-transitions in iron-bearing orthopyroxenes (centered near 425, 460, 507, and 548 nm). These absorptions are known from laboratory spectra but have been identified in the Vesta spectra of the bright howardite-/eucrite-like bright ejecta and the ejecta enriched in diogenites for the first time. These absorptions are suppressed, if existent at all, in spectra dominated by visually dark carbonaceous material, which dominates the dark-ejecta material or is mixed within the surface material of the weathered surroundings of the investigated impact craters.

The analysis of spectral properties of Vesta's surface on a local scale has provided new insight into the distribution of spectrally different materials related to HEDs. The correlation of these end-members to geological surface features and units help in understanding the processes responsible for the formation of each unit. The composition of bright ejecta material confirms the extended distribution of howardite-like breccia across Vesta's surface and is consistent with the global asymmetry with howardite/eucrite-like material dominating the equatorial regions and greater portions of diogenite-like material concentrated in the vicinity of the deeply excavated Rheasilvia basin [*De Sanctis et al.*, 2012a]. Local occurrences of diogenite-dominated material are generally related to specific impact crater features (e.g., the impact ejecta or crater material), but also can appear independent of them, which implies that impacts excavated larger blocks of diogenite-like material situated underneath the Vestan regolith. The distribution of diogenite-like material in the vicinity of the Rheasilvia and, in one case, near the Veneneia impact basin, supports the theory of diogenitic material being excavated from the deeper Vestan crust and redeposited closer to the original impact crater [*De Sanctis et al.*, 2012a]. Thus, our findings are mainly consistent with the magma ocean models proposed for Vesta's differentiation [*Takeda*, 1979]. Alternatively, local intrusions of diogenitic material cannot be fully ruled out in this stage of analysis [*Barrat et al.*, 2010; *Yamaguchi et al.*, 2011]. Further analysis of fresh surface material is necessary in order to distinguish between these two origins.

No evidence is found that the visually dark and spectrally neutral compound, which is concentrated in the material characterizing the impact craters of impact crater type 2, originates from Vesta's crust. On the contrary, our results strengthen the hypothesis of previous studies [*De Sanctis et al.*, 2012b; *McCord et al.*, 2012; *Prettyman et al.*, 2012] that the dark compound is of exogenic origin related to carbonaceous chondrites impacting Vesta's surface.

No clear correlation could be identified between albedo, band depth, and band position of pyroxene absorptions. The deepest bands are measured in diogenite-dominated regions, which, however, are characterized by an intermediate albedo like a mixture of the bright material and carbonaceous material.

Acknowledgments

We thank the Dawn engineering and science team for the development, cruise, orbital insertion, and operations of the Dawn spacecraft at Vesta. This work was performed at the DLR Institute of Planetary Research with support from the VIR visible and infrared mapping spectrometer team at the INAF Institute for Space Astrophysics and Planetology (IAPS) in Rome, Italy, JPL in Pasadena, and UCLA in Los Angeles. The VIR team is founded by ASI-INAF grant I/004/12/0.

References

Adams, J. B. (1974), Visible and near-infrared diffuse reflectance spectra of pyroxenes as applied to remote sensing of solid objects in the solar system, *J. Geophys. Res.*, *79*(32), 4829–4836, doi:10.1029/JB079i032p04829.

Ammannito, E., et al. (2012), Vesta and the HED meteorites: Comparison of spectral properties, *LPI Contrib.*, *1667*, 6326.

Ammannito, E., et al. (2013), Olivine in an unexpected location on Vesta's surface: Nature, *504*, p. 122–125.

Barrat, J.-A., A. Yamaguchi, B. Zanda, C. Bollinger, and M. Bohn (2010), Relative chronology of crust formation on asteroid Vesta: Insights from the geochemistry of diogenites, *Geochim. Cosmochim. Acta*, *74*, 6218–6231.

Beck, A. W., and H. Y. J. McSween (2010), Diogenites as polymict breccias composed of orthopyroxenite and harzburgite, *Meteorit. Planet. Sci.*, *45*(5), 850–872, doi:10.1111/j.1945-5100.2010.01061.x.

Beck, A. W., D. W. Mittlefehldt, H. Y. McSween Jr., D. Rumble III, C.-T. A. Lee, and R. J. Bodnar (2011a), MIL 03443, a dunite from asteroid 4 Vesta: Evidence for its classification and cumulate origin, *Meteorit. Planet. Sci.*, *46*, 1133–1151.

Beck, A. W., K. C. Welten, H. Y. McSween, C. E. Viviano, and M. W. Caffee (2012), Petrologic and textural diversity among the PCA 02 howardite group, one of the largest pieces of the Vestan surface, *Meteorit. Planet. Sci.*, *47*(6), 947–969, doi:10.1111/j.1945-5100.2012.01360.x.

Beck, P., J. A. Barrat, F. Grisolle, E. Quirico, B. Schmitt, F. Moynier, P. Gillet, and C. Beck (2011b), NIR spectral trends of HED meteorites: Can we discriminate between the magmatic evolution, mechanical mixing and observation geometry effects?, *Icarus*, *216*(2), 560–571, doi:10.1016/j.icarus.2011.09.015.

Binzel, R. P. (1993), Chips off Vesta: Evidence for the parent body of basaltic achondrite HED meteorites, *Meteoritics*, *28*, 323.

Binzel, R. P., M. J. Gaffey, P. C. Thomas, B. H. Zellner, A. D. Storrs, and E. N. Wells (1997), Geologic mapping of Vesta from 1994 hubble space telescope images, *Icarus*, *128*, 95–103.

Blewett, D. T., B. R. Hawke, P. G. Lucey, G. J. Taylor, R. Jaumann, and P. D. Spudis (1995), Remote sensing and geologic studies of the Schiller-Schickard region of the Moon, *J. Geophys. Res.*, *100*, 16,959–16,978.

Bowman, L. E., M. N. Spilde, and J. J. Papike (1997), Automated EDS modal analysis applied to the diogenites, *Meteorit. Planet. Sci.*, *32*, 869–875.

Burns, R. G., R. M. Abu-Eid, F. E. Huggins, J. I. Trombka, L. E. Peterson, R. C. Reedy, and J. R. Arnold (1972), Crystal field spectra of lunar pyroxenes, in *Lunar and Planetary Science Conference Proceedings*, edited by A. E. Metzger, pp. 533.

Capria, M. T., et al. (2012), Thermal inertia variations on the surface of Vesta from the Dawn data, in *Lunar and Planetary Institute Science Conference Abstracts*, p. 1863.
Clark, R. N., and T. L. Roush (1984), Reflectance spectroscopy - Quantitative analysis techniques for remote sensing applications, *J. Geophys. Res.*, *89*, 6329–6340.
Clark, R. N., C. M. Pieters, R. O. Green, J. W. Boardman, and N. E. Petro (2011), Thermal removal from near-infrared imaging spectroscopy data of the Moon, *J. Geophys. Res.*, *116,* E00G16, doi:10.1029/2010JE003751.
Cloutis, E. A., and M. J. Gaffey (1991), Spectral-compositional variations in the constituent minerals of mafic and ultramafic assemblages and remote sensing implications, *Earth Meteorites Planets*, *53*(11c), p. 11–53.
Cloutis, E. A., M. J. Gaffey, D. G. W. Smith, and R. S. J. Lambert (1990), Reflectance spectra of mafic silicate-opaque assemblages with applications to meteorite spectra, *Icarus*, *84*(2), 315–333, doi:10.1016/0019-1035(90)90041-7.
Coradini, A., D. Turrini, C. Federico, and G. Magni (2011), Vesta and Ceres: Crossing the history of the Solar System, *Space Sci. Rev.*, *163*, 25–40.
De Sanctis, M. C., et al. (2011), The VIR Spectrometer, *Space Sci. Rev.*, *163*, 329–369.
De Sanctis, M. C., et al. (2012a), Spectroscopic characterization of mineralogy and its diversity across Vesta, *Science*, *336*(6082), 697–700, doi:10.1126/science.1219270.
De Sanctis, M. C., et al. (2012b), Detection of widespread hydrated materials on Vesta by the VIR imaging spectrometer on board the Dawn mission, *Astrophys. J. Lett.*, *758*, L36.
De Sanctis, et al. (2013a), Vesta's mineralogical composition as revealed by the visible and infrared spectrometer on Dawn: Meteoritics and Planetary Science, *48*, 2166–2184.
De Sanctis, M. C., et al. (2013b), Possible detection of olivine on Vesta, *LPI Contrib.*, *1719*, 1460.
Delaney, J. S., M. Prinz, and H. Takeda (1984), The polymict eucrites, *J. Geophys. Res.*, *89*, C251–C288.
Gaffey, M. J. (1976), Spectral reflectance characteristics of the meteorite classes, *J. Geophys. Res.*, *81*, 905–920.
Gaffey, M. J. (1997), Surface lithologic heterogeneity of asteroid 4 Vesta, *Icarus, 127*, 130–157.
Gibb, E. L., M. A. DiSanti, K. Magee-Sauer, N. Dello Russo, B. P. Bonev, and M. J. Mumma (2007), The organic composition of C/2001 A2 (LINEAR). II. Search for heterogeneity within a comet nucleus, *Icarus*, *188*, 224–232.
Hinrichs, J. L., and P. G. Lucey (2002), Temperature-dependent near-infrared spectral properties of minerals, meteorites, and lunar soil, *Icarus*, *155*, 169–180.
Hinrichs, J. L., P. G. Lucey, M. S. Robinson, A. Meibom, and A. N. Krot (1999), Implications of temperature-dependent near-IR spectral properties of common minerals and meteorites for remote sensing of asteroids, *Geophys. Res. Lett.*, *26*, 1661–1664.
Hiroi, T., R. P. Binzel, J. M. Sunshine, C. M. Pieters, and H. Takeda (1995), Grain sizes and mineral compositions of surface regoliths of Vesta-like asteroids, *Icarus*, *115*(2), 374–386, doi:10.1006/icar.1995.1105.
Isaacson, P. J., and C. M. Pieters (2009), Northern Imbrium Noritic Anomaly, *J. Geophys. Res.*, *114*, E09007, doi:10.1029/2008JE003293.
Jaumann, R. (1991), Spectral-chemical analysis of lunar surface materials, *J. Geophys. Res.*, *96*, 22,793–22,807.
Jaumann, R., et al. (2012a), Investigating the origin of dark material on Vesta: Locations and geological context, in *Lunar and Planetary Institute Science Conference Abstracts*, p. 1807.
Jaumann, R., et al. (2012b), Vesta's shape and morphology, *Science*, *336*(6082), 687–690, doi:10.1126/science.1219122.
Jutzi, M., P. Gillet, J.-A. Barrat, E. Asphaug, and W. Benz (2012), The Rheasilvia impact crater as a probe of Vesta's internal structure: Results from numerical simulations, *LPI Contrib.*, *1667*, 6230.
Jutzi, M., E. Asphaug, P. Gillet, J. A. Barrat, and W. Benz (2013), The structure of the asteroid 4 Vesta as revealed by models of planet-scale collisions, *Nature*, *494*(7436), 207–210. [Available at http://www.nature.com/nature/journal/v494/n7436/abs/nature11892.html#supplementary-information.]
Keihm, S., et al. (2012), Interpretation of combined infrared, submillimeter, and millimeter thermal flux data obtained during the Rosetta fly-by of Asteroid (21) Lutetia, *Icarus*, *221*, 395–404.
Klima, R. L., C. M. Pieters, and M. D. Dyar (2007), Spectroscopy of synthetic Mg-Fe pyroxenes I: Spin-allowed and spin-forbidden crystal field bands in the visible and near-infrared, *Meteorit. Planet. Sci.*, *42*(2), 235–253, doi:10.1111/j.1945-5100.2007.tb00230.x.
Krohn, K., et al. (2012a), Geologic mapping of the Av-12 Sextlia Quadrangle of Asteroid 4 Vesta, in *Lunar and Planetary Institute Science Conference Abstracts*, p. 1901.
Krohn, K., R. Jaumann, K. Stephan, P. Schenk, F. Preusker, E. Kersten, T. Roatsch, C. A. Raymond, and C. T. Russell (2012b), Scarps and unusual crater in the Sextilia region on Vesta, *LPI Contrib.*, *1667*, 6223.
Li, J.-Y., et al. (2013), The photometric properties of Vesta in visible and near-infrared from Dawn VIR instrument, *LPI Contrib.*, *1719*, 2343.
Lucey, P. G., G. J. Taylor, and E. Malaret (1995), Abundance and distribution of iron on the Moon, *Science*, *268*, 1150–1153.
Lugmair, G. W., and A. Shukolyukov (1998), Early solar system timescales according to 53Mn-53Cr systematics, *Geochim. Cosmochim. Acta*, *62*, 2863–2886.
McCord, T. B., J. B. Adams, and T. V. Johnson (1970), Asteroid Vesta: Spectral reflectivity and compositional implications, *Science*, *168*(3938), 1445–1447, doi:10.1126/science.168.3938.1445.
McCord, T. B., et al. (2012), Dark material on Vesta from the infall of carbonaceous volatile-rich material, *Nature*, *491*(7422), 83–86. [Available at http://www.nature.com/nature/journal/v491/n7422/abs/nature11561.html#supplementary-information.]
McSween, H. Y., D. W. Mittlefehldt, A. W. Beck, R. G. Mayne, and T. J. McCoy (2011), HED meteorites and their relationship to the geology of Vesta and the Dawn mission, *Space Sci. Rev.*, *163*, 141–174.
Mittlefehldt, D. W., et al. (2012), Types and distribution of bright materials on 4 Vesta, in *Lunar and Planetary Institute Science Conference Abstracts*, p. 1680.
Mittlefehldt, D., T. J. McCoy, C. A. Goodrich, and A. Kracher (1998), Non-chondritic meteorites from asteroidal bodies, in *Planetary Materials*, edited by J. J. Papike, pp. 4-1–4-195, Mineralogical Society of America, Chantilly, Va.
Miyamoto, M., and M. E. Zolensky (1994), Infrared diffuse reflectance spectra of carbonaceous chondrites: Amount of hydrous minerals, *Meteoritics*, *29*, 849–853.
O'Brien, D. P., M. V. Sykes, and P. Tricarico (2011), Collision probabilities and impact velocity distributions for Vesta and Ceres, in *Lunar and Planetary Institute Science Conference Abstracts*, p. 2665.
Otto, K. A., et al. (2013), Mass-wasting features and processes in Vesta's south polar basin Rheasilvia, *J. Geophys. Res. Planets*, *118*, 2279–2294, doi:10.1002/2013JE004333.
Palomba, E., et al. (2013), Calibration of spectral indexes suitable for olivine detection on Vesta, *LPI Contrib.*, *1719*, 1922.
Pieters, C. M., et al. (2011a), Evidence of space weathering processes across the surface of Vesta, AGU Fall Meeting Abstracts, 22, 05.
Pieters, C. M., L. A. McFadden, T. Prettyman, M. C. de Sanctis, T. B. McCord, T. Hiroi, R. Klima, J.-Y. Li, and R. Jaumann (2011b), Surface composition of Vesta: Issues and integrated approach, *Space Sci. Rev.*, *163*, 117–139.

Pieters, C. M., et al. (2012a), Distinctive space weathering on Vesta from regolith mixing processes, *Nature*, *491*, 79–82.
Pieters, C. M., et al. (2012b), Space weathering on 4 Vesta: Processes and products, *paper presented at 43rd Lunar and Planetary Science Conference, held March 19–23, 2012 at The Woodlands, Texas. LPI Contribution No. 1659*, p. 1254.
Prettyman, T. H., et al. (2012), Elemental mapping by Dawn reveals exogenic H in Vesta's regolith, *Science*, *338*, 242–246.
Preusker, F., F. Scholten, K.-D. Matz, R. Jaumann, T. Roatsch, C. A. Raymond, and C. T. Russell (2012), Topography of Vesta from Dawn FC stereo images, in Lunar and Planetary Institute Science Conference Abstracts, p. 2012.
Reddy, V., et al. (2012a), Delivery of dark material to Vesta via carbonaceous chondritic impacts, *Icarus*, *221*, 544–559.
Reddy, V., et al. (2012b), Delivery of dark material to Vesta via carbonaceous chondritic impacts, *Icarus*, *221*(2), 544–559, doi:10.1016/j.icarus.2012.08.011.
Reddy, V., et al. (2012c), Color and albedo heterogeneity of Vesta from Dawn, *Science*, *336*(6082), 700–704, doi:10.1126/science.1219088.
Reddy, V., et al. (2012d), Photometric, spectral phase and temperature effects on 4 Vesta and HED meteorites: Implications for the Dawn mission, *Icarus*, *217*, 153–168.
Righter, K., and M. J. Drake (1997a), Formation of eucrites and diogenites on a Vesta-sized asteroid. I - Core formation, in *Lunar and Planetary Institute Science Conference Abstracts*, p. 1177.
Righter, K., and M. J. Drake (1997b), A magma ocean on Vesta: Core formation and petrogenesis of eucrites and diogenites, *Meteoritics Planet. Sci.*, *32*, 929–944.
Roatsch, T., E. Kersten, K.-D. Matz, F. Preusker, F. Scholten, R. Jaumann, C. A. Raymond, and C. T. Russell (2012), High resolution Vesta High Altitude Mapping Orbit (HAMO) Atlas derived from Dawn framing camera images, *Planet. Space Sci.*, *73*, 283–286.
Roatsch, T., E. Kersten, K.-D. Matz, F. Preusker, F. Scholten, R. Jaumann, C. A. Raymond, and C. T. Russell (2013), High resolution VESTA LAMO atlas derived from Dawn FC images, in *EGU General Assembly Conference Abstracts*, p. 1129.
Russell, C. T., and C. A. Raymond (2011), The Dawn mission to Vesta and Ceres, *Space Sci. Rev.*, *163*, 3–23.
Russell, C. T., et al. (2012a), Dawn at Vesta: Testing the protoplanetary paradigm, *Science*, *336*(6082), 684–686, doi:10.1126/science.1219381.
Russell, C. T., et al. (2012b), Dawn at Vesta: Testing the protoplanetary paradigm, *Science*, *336*, 684.
Russell, C. T., C. A. Raymond, R. Jaumann, H. Y. McSween, A. Nathues, M. C. DeSanctis, T. Prettyman, and D. S. Team (2012c), Dawn completes its mission at 4 Vesta and prepares for 1 Ceres, *LPI Contrib.*, *1667*, 6085.
Ruzicka, A., G. A. Snyder, and L. A. Taylor (1997), Vesta as the HED parent body: Implications for the size of a core and for large-scale differentiation, *Meteoritics Planet. Sci.*, *32*, 825–840.
Sandford, S. A., et al. (2006), Organics captured from comet 81P/Wild 2 by the Stardust spacecraft, *Science*, *314*, 1720.
Schenk, P., et al. (2011), The south polar structure on Vesta from Dawn: Using geologic, topographic and compositional mapping and planetary analogs to test origin models, *AGU Fall Meeting Abstracts*, *21*, 03.
Schroder, S. E., J.-Y. Li, D. W. Mittlefehldt, C. M. Pieters, M. C. de Sanctis, H. Hiesinger, D. T. Blewett, C. T. Russell, C. A. Raymond, and H. U. Keller (2012), Visible color and photometry of bright materials on Vesta, in *Lunar and Planetary Institute Science Conference Abstracts*, p. 2459.
Sierks, H., et al. (2011), The Dawn framing camera, *Space Sci. Rev.*, *163*, 263–327.
Srinivasan, G., J. N. Goswami, and N. Bhandari (1999), 26Al in eucrite Piplia Kalan: Plausible heat source and formation chronology, *Science*, *284*, 1348.
Stephan, K., C. A. Hibbitts, H. Hoffmann, and R. Jaumann (2008), Reduction of instrument-dependent noise in hyperspectral image data using the principal component analysis: Applications to Galileo NIMS data, *Planet. Space Sci.*, *56*(3-4), 406–419.
Stephan, K., et al. (2010), Dione's spectral and geological properties, *Icarus*, *206*(2), 631–652.
Sunshine, J. M., et al. (2006), Exposed water ice deposits on the surface of comet 9P/Tempel 1, *Science*, *311*, 1453–1455.
Takeda, H. (1979), A layered-crust model of a Howardite parent body, *Icarus*, *40*, 455–470.
Takir, D., J. P. Emery, H. Y. McSween, C. A. Hibbitts, R. N. Clark, N. Pearson, and A. Wang (2011), Degree of aqueous alteration in six CM/CI carbonaceous chondrites, *Meteoritics Planet. Sci. Suppl.*, *74*, 5027.
Thomas, P. C., R. P. Binzel, M. J. Gaffey, A. D. Storrs, E. N. Wells, and B. H. Zellner (1997a), Impact excavation on Asteroid 4 Vesta: Hubble Space Telescope results, *Science*, *277*(5331), 1492–1495, doi:10.1126/science.277.5331.1492.
Thomas, P. C., R. P. Binzel, M. J. Gaffey, B. H. Zellner, A. D. Storrs, and E. Wells (1997b), Vesta: Spin pole, size, and shape from HST images, *Icarus*, *128*(1), 88–94, doi:10.1006/icar.1997.5736.
Tompkins, S., and C. M. Pieters (1999), Mineralogy of the lunar crust: Results from Clementine, *Meteoritics Planet. Sci.*, *34*, 25–41.
Tosi, F., M. T. Capria, E. Ammannito, D. Grassi, E. Palomba, M. C. De sanctis, C. Russell, F. Capaccioni, J.-P. Combe, and J. Sunshine (2012a), Temperature and emissivity of local-scale features on Vesta, in *39th COSPAR Scientific Assembly. Held 14-22 July 2012, in Mysore, India. Abstract F4.7-9-12*, p. 1995.
Tosi, F., et al. (2012b), Analysis of temperature maps of selected Dawn data over the surface of Vesta, in *Lunar and Planetary Institute Science Conference Abstracts*, p. 1886.
Tosi, F., et al. (2014), Thermal measurements of dark and bright surface features on Vesta as derived from Dawn/VIR. Icarus, in press.
Williams, D. A., et al. (2012), Geologic mapping of the Av-8 Marcia Quadrangle of Asteroid 4 Vesta, in *Lunar and Planetary Institute Science Conference Abstracts*, p. 1534.
Yamaguchi, A., J.-A. Barrat, M. Ito, and M. Bohn (2011), Posteucritic magmatism on Vesta: Evidence from the petrology and thermal history of diogenites, *J. Geophys. Res.*, *116*, E08009, doi:10.1029/2010JE003753.
Yingst, R. A., et al. (2012), A global geologic map of Vesta based on high-altitude mapping orbit data, *paper presented at 43rd Lunar and Planetary Science Conference, held March 19–23, 2012 at The Woodlands, Texas. LPI Contribution No. 1659*, p. 1359.
Zambon, F., et al. (2013), Mineralogical composition of the different types of bright deposits on Vesta, *LPI Contrib.*, *1719*, 2510.
Zolensky, M. E., M. K. Weisberg, P. C. Buchanan, and D. W. Mittlefehldt (1996), Mineralogy of carbonaceous chondrite clasts in HED achondrites and the Moon, *Meteoritics Planet. Sci.*, *31*, 518–537.
Zuber, M. T., H. Y. McSween, R. P. Binzel, L. T. Elkins-Tanton, A. S. Konopliv, C. M. Pieters, and D. E. Smith (2011), Origin, internal structure and evolution of 4 Vesta, *Space Sci. Rev.*, *163*, 77–93.